Nano Research

Open Access

Review Article

Multiscale synergistic governance mechanisms and technological innovations for mixed air pollutants

Xinxin Zhang[1], Yuhan Zhou[1], Youyu Duan[2,3] ✉, Yuhan Li[1] ✉, and Fan Dong[1]

[1] *Institute for Frontier Interdisciplinary Research in Intelligence and Environment, School of Big Data, Chongqing Technology and Business University, Chongqing 400067, China*
[2] *School of Materials Science and Engineering, Chongqing Jiaotong University, Chongqing 400074, China*
[3] *Chongqing Institute of New Energy Storage Materials and Equipment, Chongqing 401120, China*

Cite this article: *Nano Research*, **2026**, *19*, 94908398. https://doi.org/10.26599/NR.2026.94908398

ABSTRACT: Atmospheric pollutants such as volatile organic compounds (VOCs), nitrogen oxides (NO_x), and ozone (O_3) pose serious threats to health and ecological systems. As air pollution evolves toward multi-pollutant coexistence, synergistic control strategies have become increasingly important. This review systematically summarizes and compares three representative synergistic systems: VOCs–NO_x, VOCs–O_3, and multi-component VOCs. For VOCs–NO_x system, the key findings highlight the dominant role of coupled redox catalytic mechanisms, strongly governed by catalyst composition, active-site regulation, and reaction conditions. Synergistic VOCs–O_3 removal is mainly achieved through photocatalytic and O_3-assisted pathways, where interfacial charge transfer and reactive oxygen species generation are critical. In complex multi-component VOC systems, integrated catalytic strategies are required to address competitive adsorption and reaction coupling, giving rise to both synergistic and inhibitory effects. Distinct from previous surveys, this review offers a unified mechanistic framework to compare these systems, emphasizes multi-scale catalyst design principles, and elucidates competitive–synergistic behaviors in realistic mixed-pollutant environments. Remaining challenges include catalyst stability, selectivity, and efficiency under multi-pollutant conditions. Future research should focus on rational catalyst design, system-level optimization, and scalable engineering implementation to advance effective synergistic air pollution control.

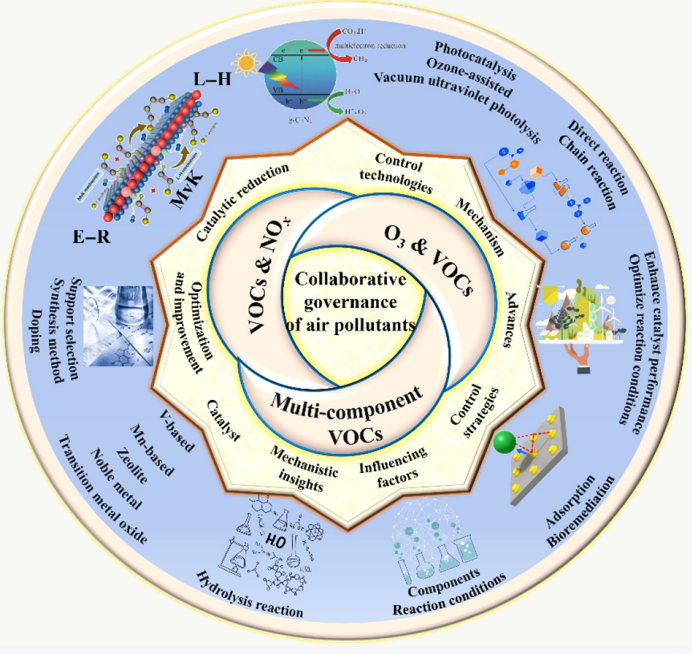

KEYWORDS: atmospheric pollutants, volatile organic compounds, nitrogen oxides, ozone, synergistic control

1 Introduction

The rapid advancement of industrialization and urbanization has intensified atmospheric pollution, posing a global environmental and health challenge. According to WHO estimates, air pollution contributes to over 7 million premature annual deaths from conditions including cancer and stroke, ranking as the thirteenth leading global mortality risk factor. Most regions fail to meet WHO air quality standards, with some exceeding limits by more than tenfold, underscoring severe environmental health risks [1–3]. Atmospheric pollutants impact human health through multiple pathways. Ozone (O_3), as a potent oxidant, reacts with biological molecules. Acute high-concentration exposure induces symptoms including cough and chest pain, potentially progressing to pulmonary impairment or mortality [4, 5]. Volatile organic

Received: November 24, 2025; **Revised:** December 29, 2025
Accepted: January 1, 2026

✉Address correspondence to Youyu Duan, youyuduan@cqjtu.edu.cn; Yuhan Li, liyh@ctbu.edu.cn

compounds (VOCs) manifest multi-system toxicity, where chronic exposure may cause neurological impairment and hematopoietic suppression, with certain aromatic compounds exhibiting genotoxicity [6–8]. As crucial precursors, VOCs and nitrogen oxides (NO_x) undergo photochemical reactions forming O_3 and secondary organic aerosols [9–11]. Elevated O_3 concentrations induce foliar damage, photosynthetic inhibition, and agricultural yield reduction [12, 13]. NO_x deposition generates nitrate compounds, accelerating soil acidification and plant damage [13–15]. Industrial VOCs (e.g., ethylene, propylene) demonstrate flammability hazards, while persistent organic pollutants like benzene, toluene, ethylbenzene, and xylene (BTEX) bioaccumulate through trophic transfer, threatening ecosystem integrity [16–18].

Atmospheric pollutants originate from diverse sources, primarily including industrial emissions, transportation, biomass burning, and biogenic origins [19]. As key pollutants, VOCs and NO_x emissions exhibit significant spatial heterogeneity and transport differentials [20]. NO_x undergoes secondary transformation to generate O_3 and nitrate aerosols, capable of regional to continental-scale transport, serving as major contributors to photochemical smog and acid rain [21]. The transport capacity of VOCs depends on their atmospheric lifetime: Short-lived components (e.g., isoprene) affect local areas, while long-lived species (e.g., methane and halocarbons) undergo intercontinental transport and contribute to global warming [22, 23]. Both are concentrated in anthropogenic emission hotspots and biogenically active regions, acting as core precursors for O_3 and secondary particulate matter, driving global background ozone increase and transboundary fine particle transport [24, 25]. Current VOCs control technologies mainly include thermal combustion [26], catalytic oxidation [27], and biological treatment [28]. Catalysts for VOCs combustion require high selectivity, activity, thermal stability, and poisoning resistance to avoid generating highly toxic by-products. Compared to thermal combustion, catalytic oxidation enables efficient VOCs conversion at lower temperatures, completely oxidizing them to carbon dioxide (CO_2) and water (H_2O), offering advantages of high efficiency, energy savings, and environmental friendliness, thereby emerging as a mainstream VOCs elimination technology [29, 30]. Photocatalytic technology, powered by renewable solar energy, has garnered increasing attention due to its mild reaction conditions, energy efficiency, and non-toxic nature [31, 32]. Sun et al. [33] developed an R-$BiVO_4$/WO_3/TiO_2 nanotubes (TNTs) catalyst demonstrating a 28-fold enhancement in photocurrent intensity, achieving complete toluene degradation within 50 min, exhibiting excellent visible-light photocatalytic activity and durability. Xu et al. [34] constructed a Co-Vo-Cu catalyst achieving 99% toluene degradation under visible light in 50 min, releasing 637 ppm CO_2, indicating that atomic-scale regulation of reaction pathways enables efficient deep mineralization of pollutants with low energy consumption and high cleanliness. Furthermore, Hu et al. [35] achieved 99.2% toluene mineralization by constructing Sn–O electron channels, demonstrating efficient multi-reactive oxygen species synergy and good environmental adaptability. However, photocatalytic technology still faces key challenges including poor stability, susceptibility to deactivation, low quantum efficiency, rapid charge carrier recombination, and insufficient active sites. NO_x elimination primarily employs selective catalytic reduction with ammonia (NH_3-SCR), where ammonia (NH_3) serves as the reductant to convert NO_x into nitrogen (N_2) and H_2O ($4NH_3 + 4NO + O_2 \rightarrow 4N_2 + 6H_2O$) within a temperature range of 150–450 °C, with N_2O ($4NH_3 + 4NO + 3O_2 \rightarrow 4N_2O + 6H_2O$) as a by-product [36, 37], though it remains vulnerable to alkali/heavy metal poisoning. O_3 control can be achieved through catalytic decomposition [38], ultraviolet (UV) photolysis [39], or precursor control. Existing air pollution control technologies still face limitations in conversion efficiency, catalyst susceptibility to poisoning/deactivation, and secondary pollution risks. Zhang et al. [40] reported a $Mn_aCo_bNiO_x$ catalyst achieving over 90% synergistic removal of NO_x and benzene (C_6H_6) between 100 and 270 °C. Gervasini et al. [41] observed that O_3 synergy with Ba-CuO-Cr_2O_3/Al_2O_3 enhanced C_6H_6 conversion to 98%, but the degradation efficiency for chlorinated VOCs like C_2HCl_3 remained below 40%. Wang et al. [42] developed a 0.96($AuPd_{1.92}$)/Co_3O_4 catalyst demonstrating excellent low-temperature activity (ignition temperature, T_{90} = 180 and 187 °C for toluene and o-xylene oxidation, respectively), though challenges like water vapor sensitivity persist.

Over recent decades, the development of high-efficiency treatment technologies has been a central research focus in environmental engineering and catalytic science, aiming to systematically enhance air pollution control performance. Within this context, synergistic control strategies have progressively replaced conventional single-pollutant approaches, emerging as a critical direction in air pollution mitigation. These integrated approaches demonstrate significant advantages by enabling simultaneous removal of multiple pollutants, reducing energy consumption, minimizing secondary pollution, and enhancing reaction efficiency, with substantial breakthroughs achieved in both fundamental research and practical applications. This review systematically consolidates recent advances in synergistic control of mixed air pollutants, with particular emphasis on three key areas (Fig. 1): synergistic catalytic elimination of NO_x and VOCs, cooperative control mechanisms for VOCs and O_3, and efficient synergistic degradation of complex multi-component VOCs. Through comparative analysis of treatment technologies, mechanistic investigation of reaction pathways, rational catalyst design strategies, and in-depth discussion of performance influencing mechanisms, this work aims to provide theoretical foundations and technical support for developing high-performance synergistic control systems, thereby facilitating the translation of fundamental research into practical applications.

2 Synergistic management of VOCs and NO_x

VOCs and NO_x serve as critical precursors for the formation of $PM_{2.5}$ and O_3. Under solar radiation, they participate in photochemical reactions that generate O_3 and photochemical smog, posing significant threats to atmospheric environment and human health [9–11]. Although catalytic oxidation of VOCs and selective catalytic reduction (SCR) of NO_x are often investigated separately, many catalysts exhibit activity toward both types of reactions, with their performance strongly dependent on the acidity and redox properties of the catalysts [10–12]. This mechanistic similarity offers a promising foundation for developing highly efficient catalytic systems capable of synchronously eliminating VOCs and NO_x.

2.1 Mutual reaction mechanism

VOCs and NO_x exhibit significant synergistic interactions during catalytic processes. On one hand, VOCs undergo complex

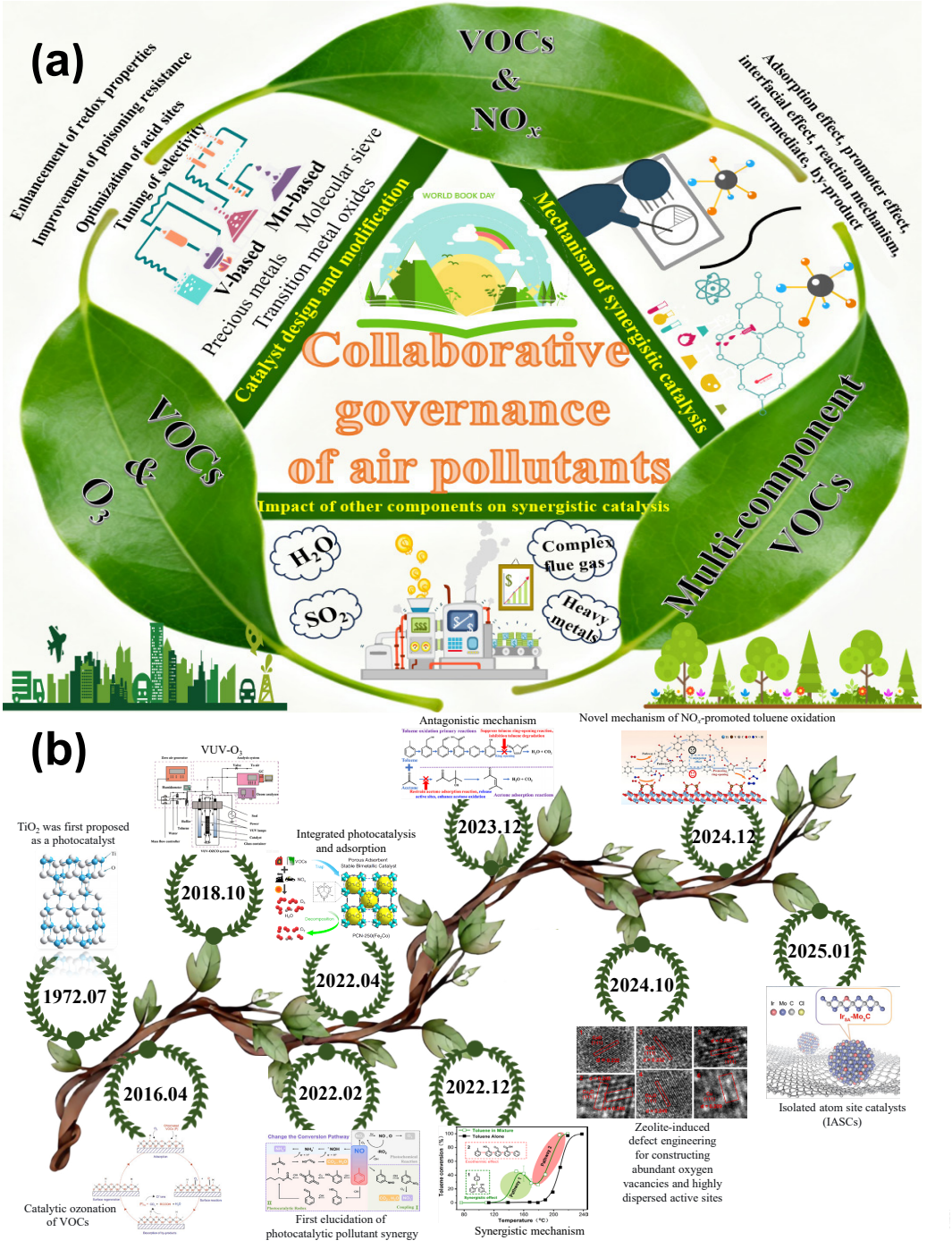

Figure 1 (a) Synergistic control of multi-pollutant mixtures. (b) The development of synergistic control technologies and nanocatalysts. The figures are arranged in chronological order: Adapted with permission from Ref. [43], © Springer Nature Limited 1972. Adapted with permission from Ref. [44], © Elsevier B.V. 2016. Adapted with permission from Ref. [45], © Elsevier B.V. 2018. Adapted with permission from Ref. [46], © Elsevier B.V. 2022. Adapted with permission from Ref. [47], © Dong et al. 2022. Adapted with permission from Ref. [48],© American Chemical Society 2022. Adapted with permission from Ref. [49], © American Chemical Society 2024. Adapted with permission from Ref. [50], © Elsevier B.V. 2024. Adapted with permission from Ref. [51], © Elsevier B.V. 2024. Adapted with permission from Ref. [52], © Wiley-VCH GmbH 2025.

photochemical reactions under light irradiation. Unsaturated VOCs (e.g., alkenes, aromatics) absorb photon energy, triggering intramolecular electron transitions to generate reactive radicals (e.g., benzyl radicals and hydrogen atoms from toluene photolysis) [53]. Simultaneously, NO_2 photodissociation produces NO and O atoms, with the latter reacting with O_2 to form O_3 [54]. Radicals derived from VOCs photolysis (e.g., alkyl and acyl radicals) accelerate NO-to-NO_2 conversion, thereby promoting O_3 formation [55]. Furthermore, these radicals react with NO_x to form secondary organic aerosols (SOAs), actively participating in SOA nucleation and growth processes, significantly impacting particulate matter concentrations and air quality [56]. On the other hand, oxidative intermediates of VOCs can serve as additional reductants to enhance SCR reactions of NO_x, while their deep oxidation

effectively reduces carbonaceous deposits that cause SCR active site poisoning [57]. Although VOCs oxidation consumes lattice oxygen and suppresses NO oxidation, the presence of aromatic hydrocarbons conversely inhibits toxic NO_2 generation while promoting NO conversion to NO_2^-, NO_3^-, and N_2 (Fig. 2(a)) [58]. Notably, competitive adsorption occurs between toluene and NH_3 on acid sites: slightly promoting NO_x conversion at low temperatures (< 175 °C) while significantly suppressing NH_3-SCR reactions at elevated temperatures, with toluene oxidation intermediates (e.g., benzoic acid) occupying redox-active sites and consequently affecting SCR processes [59].

Meanwhile, NO_x plays a crucial role in promoting the deep oxidation of VOCs. Gong et al. [57] demonstrated that VMoTi active sites effectively catalyzed the further conversion of incomplete oxidation intermediates (e.g., benzoic acid) generated at VPO sites into CO_2 and H_2O, significantly enhancing mineralization efficiency. The synergistic effect between dual active sites simultaneously reduced the ignition temperature for complete VOCs oxidation and broadened the operational temperature window (Fig. 2(b)). More importantly, NO_2 generated from NO oxidation serves as a strong oxidant, establishing a dynamic "lattice oxygen activation-replenishment" cycle that effectively compensates for lattice oxygen consumed during VOCs reactions. This mechanism prevents catalyst deactivation and ensures continuous supply of active oxygen species, thereby significantly promoting ring-opening reactions and deep oxidation of aromatic hydrocarbons [58]. Furthermore, Gan et al. [59] confirmed that reactive oxygen species (e.g., $\cdot O^-$, $\cdot O_2^-$) generated from NO_x decomposition at redox sites directly participate in toluene oxidation. In the optimized Ce2Si1 catalyst, owing to its balanced physicochemical properties, the inhibitory effect of NO_x on toluene oxidation was significantly mitigated, enabling efficient synergistic elimination across a broad temperature window of 300–375 °C.

In synergistic control systems for VOCs and NO_x, the elimination processes are not independent but achieve enhanced efficiency through profound interplays. These interactions enable VOCs to promote the deep conversion of NO_x into harmless products, while NO_x plays a critical role in maintaining sustained catalytic activity. These mechanisms provide fundamental theoretical insights and diverse technical pathways for designing efficient and stable multipollutant control catalysts.

2.2 Collaborative mechanism

Catalytic oxidation of VOCs and SCR of NO_x are inherently linked in their reaction pathways and catalytic functional requirements: both processes rely on bifunctional catalysts containing acid sites (for adsorbing/activating reactant molecules) and redox sites (for regulating electron transfer processes) [60–62]. Furthermore, their coincident operational temperature windows [63] enable simultaneous efficient VOCs oxidation and NO_x reduction. These fundamental similarities establish the feasibility for developing integrated removal systems targeting both pollutants.

2.2.1 *Catalytic redox mechanisms*

In synergistic catalytic systems for NO_x and VOCs, redox mechanisms form the core of the reactions, wherein the Mars-van Krevelen (MvK) mechanism (Fig. 2(c)) and pathways derived from SCR, including the Eley-Rideal (E-R) and Langmuir-Hinshelwood (L-H) mechanisms (Fig. 2(d)), play predominant roles [64, 65] (Table 1).

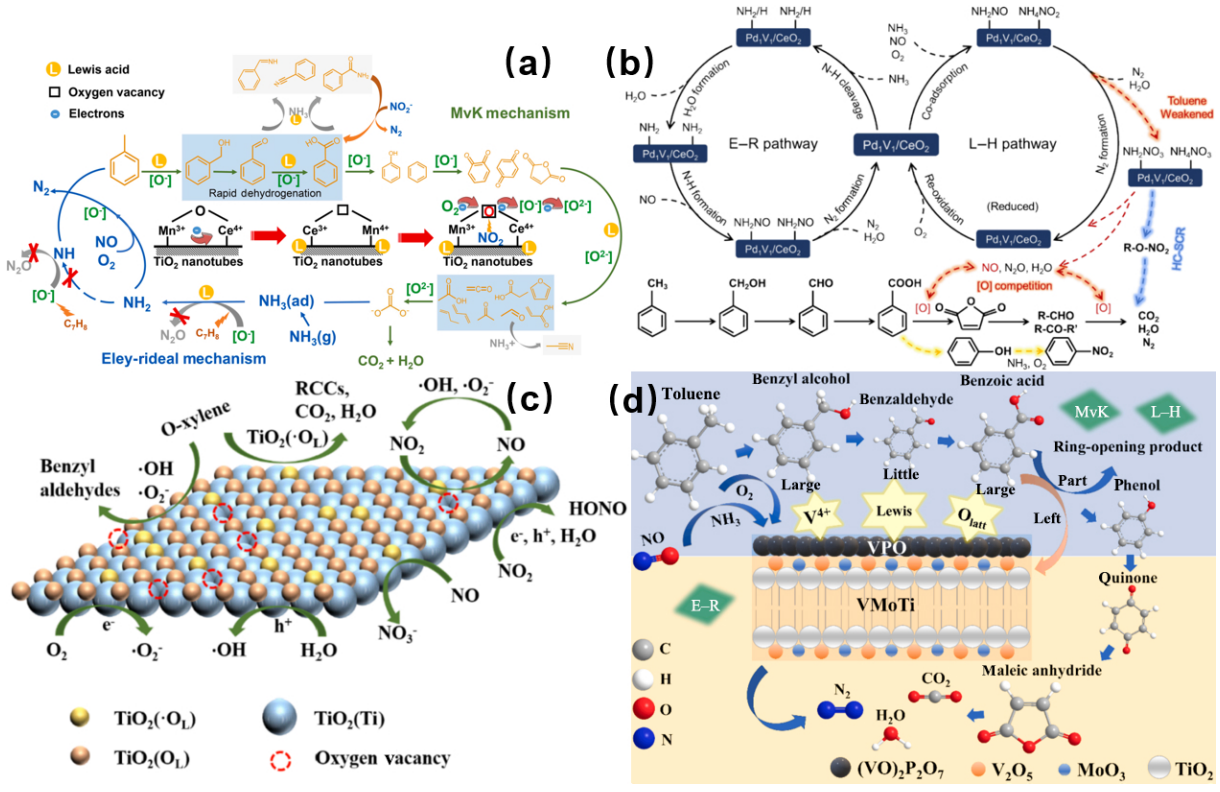

Figure 2 (a) Schematic diagram of the Mars–van Krevelen (MvK) mechanism. Reproduced with permission from Ref. [67], © Elsevier B.V. 2023. (b) Schematic diagram of the Eley–Rideal (E–R) and Langmuir–Hinshelwood (L–H) mechanisms. Reproduced with permission from Ref. [69], © American Chemical Society 2024. (c) PCO mechanism in the o-xylene/NO/air reaction system. Reproduced with permission from Ref. [58], © Elsevier B.V. 2022. (d) Reaction pathway of the VPO-VMoTi tandem catalytic filter for simultaneous removal of NO_x and VOCs. Reproduced with permission from Ref. [57], © Elsevier B.V. 2025.

Table 1 Key characteristics and roles of MvK, E–R, and L–H mechanisms in synergistic VOCs-NO_x removal

Mechanism	Conditions and key features	Role
MvK [57, 67]	Requires redox-active catalyst with mobile lattice oxygen. VOCs consume lattice O, creating vacancies replenished by gaseous O_2/NO_2.	Drives deep oxidation of VOCs; NO_2 aids oxygen transfer, sustaining catalytic activity and inhibiting deactivation.
E–R [69]	Involves reaction between a gas-phase molecule (e.g., NO) and an adsorbed species (e.g., NH_2 from NH_3).	Dominates the NH_3-SCR pathway for NO_x reduction; enables direct reaction of gaseous VOCs/intermediates with adsorbed NO_x.
L–H [69]	Requires co-adsorption of reactants (e.g., NH_4^+ and NO_x adspecies) on adjacent surface sites; surface reaction is rate-limiting.	Promotes surface-coupled reactions in SCR, enhancing N_2 selectivity; mitigates competitive poisoning in VOCs-NO_x co-adsorption.

In the MvK mechanism, VOCs initially react with lattice oxygen on the catalyst surface, generating oxygen vacancies. These vacancies serve as crucial intermediate states in the catalytic process, providing active sites for the subsequent adsorption and activation of gaseous oxygen or oxygen atoms [2]. To replenish the surface oxygen vacancies, gaseous oxygen or oxygen atoms from the system adsorb onto the catalyst surface and undergo a series of reactions to regenerate the reduced active components of the catalyst. This process ensures a continuous supply of reactive oxygen, thereby sustaining the catalytic reaction [66]. The sequence begins with the adsorption and activation of VOCs on Lewis acid sites, followed by nucleophilic attack by lattice oxygen on the intermediates, driving their stepwise oxidation and initiating aromatic ring opening, ultimately yielding CO_2. Simultaneously, the consumed lattice oxygen is replenished via the adsorption, activation, and incorporation of gaseous oxygen at the oxygen vacancy sites, achieving catalyst regeneration through a redox cycle. Notably, the by-product NO_2, acting as a strong oxidant, can directly participate in the transfer and replenishment of lattice oxygen via the pathway NO_2 (ads) → O^- (ads) → O^{2-} (lattice), further promoting the deep oxidation of VOCs and enhancing the reaction cycle [67]. In the E-R pathway, gaseous VOCs directly react with adsorbed NO_x species. Studies have shown that NH_3 first adsorbs on Lewis acid sites of the catalyst, where it is oxidatively dehydrogenated to form amino species (NH_2). The activated NH_2 then reacts with gaseous NO to form a nitrosamine intermediate (NH_2NO), which subsequently decomposes into N_2 and H_2O. In the Langmuir-Hinshelwood (L-H) pathway, both NO_x and VOCs must be co-adsorbed on adjacent active sites to undergo surface reactions. Here, NH_4^+ formed from NH_3 adsorbed on Brønsted acid sites reacts with nitrate/nitrite complexes generated from NO adsorbed on Lewis acid sites, forming NH_4NO_3 on the catalyst surface, which then decomposes into N_2 and H_2O [68]. Furthermore, it has been reported that by modulating lattice oxygen mobility and the surface electronic structure, it is possible to suppress the over-oxidation of key intermediates (such as nitrites), thereby significantly enhancing the performance of synergistic catalysis [69].

The MvK mechanism facilitates the deep oxidation of VOCs and catalyst regeneration through a lattice oxygen-oxygen vacancy cycle, while the E-R and L-H pathways drive the targeted reduction of NO_x via gaseous radical interception and surface ion coupling, respectively; the synergy among these three constructs a dynamic catalytic network enabling the highly efficient co-conversion of NO_x and VOCs.

2.2.2 *Other mechanisms*

In integrated VOCs and NO_x abatement systems, a variety of mechanisms operate alongside catalytic redox pathways. Absorption removes pollutants via chemical or physical dissolution into a solvent; biological treatment relies on microorganisms that metabolize pollutants as energy sources [61]; adsorption employs physical or chemical interactions on solid surfaces to capture contaminants [70]; condensation separates VOCs by lowering the temperature, with partial co-removal of NO_x achievable under certain conditions [71]; membrane separation utilizes selective permeation through porous or dense membranes to isolate pollutants [72]; plasma-catalysis coupling applies non-thermal plasma (NTP) to cleave recalcitrant VOCs molecules (e.g., chlorobenzene → ·CH_3) while generating reactive species (e.g., ·O/·OH) *in situ*, significantly reducing the activation energy required for oxidizing halogenated compounds [73]; photocatalysis exploits electron-hole pairs generated in semiconductors (e.g., TiO_2) upon photoexcitation, enabling simultaneous reduction of NO_x by conduction band electrons and oxidation of VOCs by valence band holes [74].

By integrating complementary processes-including directional transport across multiphase media (absorption/adsorption/condensation/membrane separation), biological metabolism, and energy field activation (e.g., plasma cracking and photoinduced charge carriers)-this synergistic governance system achieves end-to-end regulation of VOCs and NO_x, from enrichment and separation to deep conversion. It thus offers a systematic strategy beyond single-mode redox pathways for treating complex industrial waste gases.

2.3 Catalyst design

In mixed VOCs and NO_x systems, their removal processes are markedly non-independent; rather, they exhibit synergistic enhancement through complex and profound interaction mechanisms. From a functional perspective, VOCs can promote the deep conversion of NO_x into harmless products such as N_2-either by providing reactive sites or participating in intermediate transformations-thereby significantly improving NO_x removal efficiency. Concurrently, NO_x contributes to maintaining the long-term stable activity of the catalyst, primarily by modulating the surface electronic state and suppressing by-product formation, thereby furnishing the necessary catalytic environment for efficient VOCs degradation. Based on their mutual reaction mechanisms and synergistic catalytic behavior, it is established that constructing suitable acid and redox sites on the catalyst surface is key to achieving synergistic elimination of VOCs and NO_x.

2.3.1 *Catalyst types*

Vanadium-based (V-based) catalysts have achieved commercial application owing to their superior stability, abundant acid sites, and strong resistance to sulfur poisoning. However, their weak oxidation capacity often leads to the accumulation of partial oxidation by-products and, in the case of chlorinated VOCs (CVOCs), may promote the formation of highly toxic dioxins. Manganese-based (Mn-based) catalysts, representative transition metal oxides, have attracted significant attention due to their remarkable low-temperature activity (< 200 °C) and cost-

effectiveness. Nonetheless, they suffer from challenges such as active component leaching, poisoning-induced deactivation, and insufficient thermal stability. Zeolite catalysts enhance reaction selectivity through their rigid framework structure and shape-selective catalytic properties; however, their high cost and complex synthesis procedures substantially limit exploration of large-scale applications (Table 2).

V-based catalysts. V-based catalysts hold significant importance in industrial waste gas treatment, particularly demonstrating notable performance and stability in the reduction of NO_x under complex flue gas conditions. In commercial SCR catalysts, the existing form and valence state of vanadium profoundly influence its catalytic activity. While these catalysts also exhibit certain capability in the catalytic destruction of chlorinated volatile organic compounds (CVOCs), they display evident limitations in the catalytic oxidation of VOCs within coal-fired flue gas purification scenarios. On one hand, their relatively low oxidation efficiency toward VOCs often impedes complete conversion into harmless substances; on the other hand, the reaction process tends to yield a considerable amount of by-products [75]. This not only diminishes the selectivity toward desired products but may also introduce secondary pollution, thereby posing challenges for V-based catalysts in achieving the synergistic and efficient removal of both NO_x and VOCs.

To address the aforementioned issues, existing studies have explored the introduction of a second transition metal as an effective strategy. Lin et al. [76] constructed V-Cu dual-metal sites on TiO_2, modulating the active site structure to facilitate electron

Table 2 VOCs-NO_x synergistic performance summary.

Catalyst [Ref.]	Preparation method	VOCs conversion temperature (°C) (efficiency (%))	NO_x conversion temperature (°C) (efficiency (%))	Selectivity (%)
V_5Mo_5Ti [80]	Conventional impregnation method	300 (> 95)	200–400 (100)	>90 (N_2)
5% V/Ti [51]	Wet impregnation method	250	200–350	~ 90 (CO_2)
MnO_x@CeO_2@MgO [83]	Two-step method	300 (> 80)	300 (86)	≥ 93 (N_2) 80 (CO_2)
MnO_2 nanorod [85]	Hydrothermal method	275 (> 90)	125–300 (> 60)	—
MnO(0.4)-CeO_2 [63]	Hydrothermal method	300 (> 90)	125–300 (> 80)	> 85 (N_2)
Mn-Cu/SBA-15 [95]	Hydrothermal method	250 (100)	300 (> 70)	—
Cu/Beta@CeO_2 [96]	Self-assembly method	300 (> 90)	250–400 (> 80)	> 80 (CO_2)
Cr-CeO_2 [97]	Co-precipitation method	330 (> 90)	240 (> 90)	90 (N_2)
VPO-VMoTi [57]	Layer-by-layer drop-coating method	250–400 (~ 100)	250–400 (~ 100)	> 95 (N_2)
TiO_2 (anatase) [58]	—	(100)	(18.20)	—
Ce2Si1 [59]	Reverse co-precipitation method	300–375 (> 90)	300–375 (> 90)	> 95 (N_2)
Co-MnO_x [87]	Sol-gel method	≥ 180 (> 90)	105–275 (> 90)	> 75 (N_2)
Cu-MnO_2 [88]	Precipitation method	260 (~ 98.5)	260 (68)	> 50 (N_2) 80 (CO_2)
Al^{3+}-CeO_2 [98]	Homogeneous co-precipitation method	274 (> 80)	185 (30)	94 (N_2)
$In(OH)_3$ [46]	Precipitation method	(65.50)	(100)	3.7 (N_2O)
$NiMn_2O_4$-CeO_2 [89]	Precipitation method	210 (90)	100–250 (> 80%, 100% in 100 °C)	—
V1-Cu_5/TiO_2 [76]	Impregnation method	257 (> 90)	(> 97)	~ 100 (N_2)
Fe-MnO_2-F&R [86]	Hydrothermal method	170 (> 90)	170 (> 80)	—
Fe-MnO_2@TiO_2 [84]	Hydrothermal method	188–316 (> 90)	188–316 (> 90)	~ 100 (N_2)
PdV/TiO_2 [82]	Sol-gel method	(> 90)	(> 90)	—
CuCeTi [62]	Homogeneous co-precipitation method	257 (> 90)	(> 90)	~ 100 (N_2) >95 (CO_2)
CeO_2-TiO_2 [99]	Homogeneous co-precipitation method	300 (~ 100)	(> 90)	> 96 (N_2) ~ 100 (CO_2)
Co-$SmMn_2O_5$ [92]	Hydrothermal method	270 (> 90)	160–300 (> 80)	> 80 (N_2) ~ 100 (CO_2)
MnCe/TNT [67]	Hydrothermal method combined with impregnation method	196 (> 90)	182–300 (> 80)	> 90 (CO_2)
Pd1V1/CeO_2 [69]	Hydrothermal self-assembly method	238 (90)	230 (90)	98 (N_2) 98 (CO_2)
NbmCeO_x [100]	Homogeneous co-precipitation method	> 210 (> 90)	170–390 (> 90)	> 85 (N_2) >80 (CO_2)
Ag-Mn/HZSM-5 [90]	Wet impregnation method	293–400 (> 60)	293–400 (> 90)	> 90 (N_2) >90 (CO_2)
$V_{0.5}Mn_5Co_5$ [91]	Oxalic acid precipitation method	260 (92)	180–300 (> 95)	≥ 80 (N_2)
Cu_5-VWT [81]	Wet impregnation method	350 (> 99)	—	> 99 (CO_2)

transfer and the formation of reaction intermediates. This significantly enhanced the synergistic removal efficiency of toluene and NO_x, while improving catalyst stability and anti-poisoning ability. The mechanism is attributed to the strong interaction between Cu and V, promoting electron transfer from Cu to adsorbed oxygen and generating reactive oxygen species (O_2^-), thereby enhancing toluene oxidation activity. Gong et al. [57] designed a tandem catalytic filter with VPO and VMoTi layered loading, achieving highly efficient synergistic removal of NO_x and toluene (close to 100%) within 200–400 °C, and reducing the toluene ignition temperature from 320 to 170 °C (Figs. 3(a)–3(b)). The catalyst exhibited excellent low-temperature activity and sulfur resistance stability, with C1 selectivity increased by nearly 200%, indicating significantly enhanced mineralization. It maintained stable performance for 100 h in the presence of SO_2 and water vapor. Vanadium-tungsten-titanium (VW/Ti) catalysts, as a mature SCR catalyst, possess excellent anti-poisoning capability, acidity, and redox properties, demonstrating potential in the synergistic catalysis of VOCs and NO [77–79]. Lian et al. [75] investigated metal modification of VW/Ti catalysts and found that excessive metal loading adversely affected performance, while composite metal modification was less effective than single or dual-metal systems. Among them, Cu-modified and Fe-modified catalysts performed best in the synergistic removal of NO and VOCs, with the Cu-modified catalyst achieving 89.9% NO conversion at 380 °C and average removal rates of 97.1% and 92.7% for benzene and toluene, respectively. Huang et al. [80] studied the synergistic removal of chlorobenzene (CB) and NO over a V_5Mo_5Ti catalyst. They found that its oxidation capacity was limited, with some CB only oxidized to dichloromaleic anhydride without further mineralization, resulting in low CO_2 selectivity. Additionally, chlorine species (e.g., CCl_4 and C_2Cl_4) accumulated on the catalyst surface, leading to deactivation. Liu et al. [51] systematically investigated the effect of different V loadings on the structure and performance of V/Ti catalysts, finding that the 5% V/Ti catalyst exhibited optimal active site distribution and redox capacity. Through *in situ* infrared (IR) and gas chromatography-mass spectrometry (GC-MS) analysis, a novel mechanism for NO_x-promoted toluene oxidation was proposed: NO_x attacks the toluene side chain to form benzohydroxamic acid, which polarizes the aromatic ring via a conjugation effect, reducing the ring-opening energy barrier and accelerating the reaction (Figs. 3(c) and 3(d)). Xiao et al. [81] developed a Cu-vanadium-tungsten-titanium (Cu-VWT) catalyst bifunctional catalyst, where highly dispersed V and Cu sites predominantly govern NO reduction and VOCs oxidation, respectively (Fig. 3(e)). The catalyst exhibited high surface-reactive

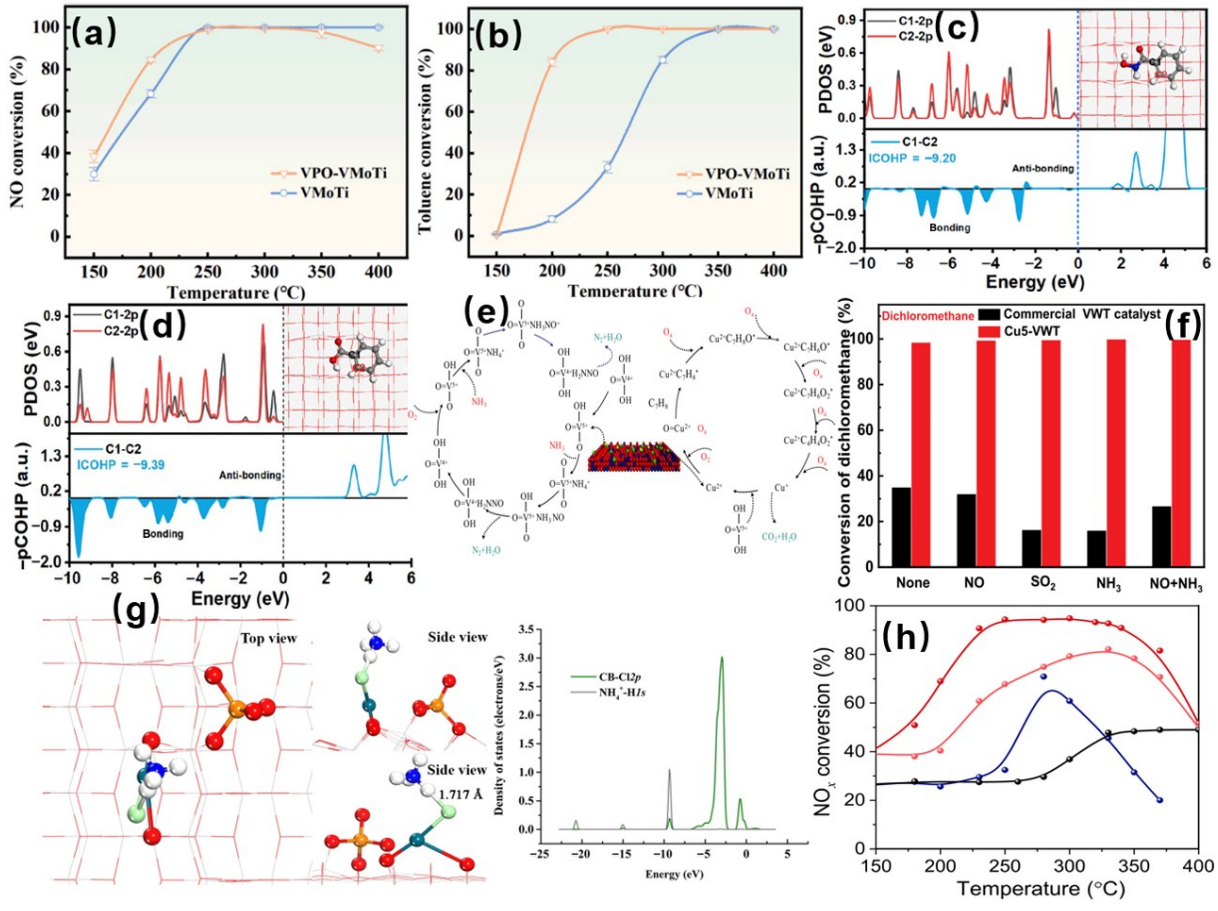

Figure 3 Removal behaviors of NO_x and VOCs over the VPO-VMoTi tandem catalytic filter and VMoTi catalytic filter: (a) NO conversion and (b) toluene conversion. Reproduced with permission from Ref. [57], © Elsevier B.V. 2025. Projected density of states (PDOS) and crystal orbital Hamilton population (COHP) analyses for (c) benzoic acid and (d) benzohydroxamic acid. Reproduced with permission from Ref. [51], © Elsevier B.V. 2024. (e) Mechanism for the synergistic removal of toluene and NO over the Cu-VWT catalyst. (f) Dichloromethane conversion over different catalysts under simulated flue gas conditions. Reproduced with permission from Ref. [81], © American Chemical Society 2023. (g) Adsorption behavior of NH_4^+ on Brønsted acid sites. Reproduced with permission from Ref. [82], © Elsevier B.V. 2021. (h) NO_x conversion over different catalysts. Reproduced with permission from Ref. [69], © American Chemical Society 2024.

oxygen content and balanced redox properties, effectively suppressing polycyclic aromatic hydrocarbon (PAH) formation and achieving efficient synergistic removal of VOCs and NO_x, with a total VOCs removal rate of 97.9% (Fig. 3(f)). Li et al. [82] prepared PdV/TiO_2 catalysts by tuning the atomic ratio of Pd to V, which demonstrated excellent synergistic CB/NO removal efficiency and CO_2/N_2 selectivity within 300–400 °C. The study revealed that NO_2 acted as an oxidant participating in CB oxidation and regenerating oxygen vacancies, while NH_3 reacted with Cl species adsorbed on Pd sites to form NH_4Cl, inhibiting CB oxidation (Fig. 3(g)). Chu et al. [69] employed a Pd-V dual single-atom catalyst for simultaneous toluene oxidation and NO_2 reduction, compressing the temperature window for > 80% NO_2 conversion to 152 °C (Fig. 3(h)), significantly outperforming single-atom catalysts. Both CO_2 and N_2 selectivity reached 98%, achieving near-complete mineralization. The broad temperature window, high selectivity, high stability, and anti-poisoning performance provide a new paradigm for synergistic control of multiple pollutants.

Mn-based catalysts. Mn-based catalysts demonstrate superior performance in the simultaneous reduction of NO_x and oxidation of VOCs, owing to their unique physicochemical properties. Their excellent redox capability primarily stems from the multivalent nature of manganese, which facilitates flexible transitions between Mn^{2+}, Mn^{3+}, and Mn^{4+}, thereby promoting electron transfer during reactions. To enhance the synergistic removal of VOCs and NO_x in sulfur-containing flue gas, researchers have optimized Mn-based catalysts through structural and compositional design. Pan et al. [83] constructed a core–shell $MnO_x@CeO_2@MgO$ catalyst, in which the MgO shell preferentially reacts with SO_2 to form $MgSO_4$, effectively protecting the inner MnO_x and CeO_2 active sites. Under conditions of 300 ppm SO_2 and 300 °C, the conversion rates of NO_x and CB remained above 80%, demonstrating excellent sulfur resistance stability (Fig. 4(a)). Similarly, Lin et al. [84] developed a $Fe\text{-}MnO_2@TiO_2$ core–shell catalyst, in which the TiO_2 shell inhibits SO_2 deposition and oxidizes SO_2 to surface sulfates via unsaturated Ti sites and bridge hydroxyl groups, thereby protecting the internal active sites and enhancing catalyst stability (Fig. 4(b)). Morphology control and crystal phase design are also key strategies for improving the performance of Mn-based catalysts. Jia et al. [85] compared the catalytic performance of MnO_x nanorods and nanocuboids, finding that the former achieved 85% synergistic removal of NO and toluene at 275 °C due to a higher Mn^{4+} ratio and superior redox capability. MnCe solid solution catalysts significantly lower the oxidation temperature of VOCs due to their enhanced redox properties. Gan et al. [63] reported that the $MnO_x(0.4)–CeO_2$ solid solution achieved a good balance between

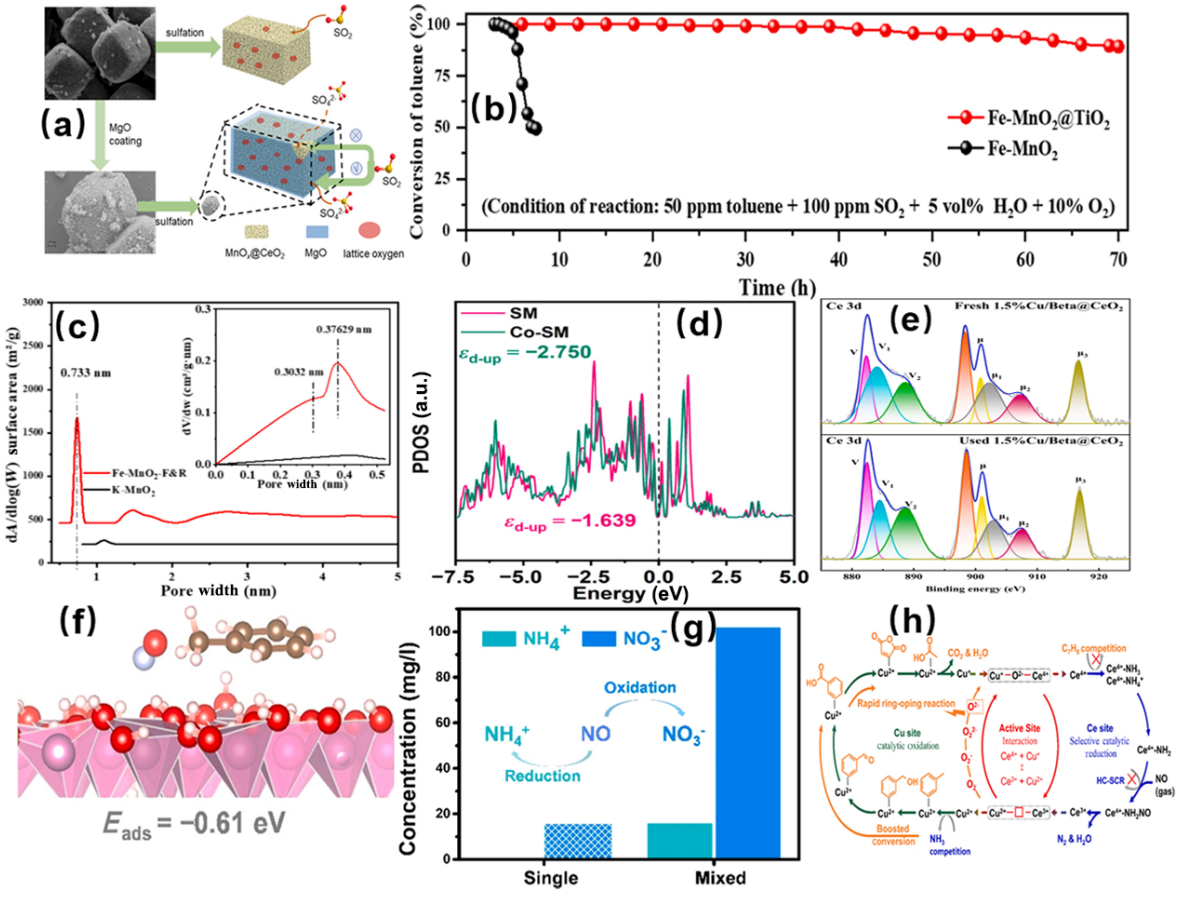

Figure 4 (a) Effect of the MgO shell on the SO_2 resistance of the $MnO_x@CeO_2@MgO$ catalyst. Reproduced with permission from Ref. [83], © Elsevier B.V. 2024. (b) Sulfur and water resistance stability of $Fe\text{-}MnO_2@TiO_2$ at 220 °C. Reproduced with permission from Ref. [84], © Elsevier B.V. 2024. (c) Pore size distribution of K-MnO_2-120 and Fe-MnO_2-F&R. Reproduced with permission from Ref. [86], © American Chemical Society 2024. (d) Projected density of states (PDOS) of the Mn-Mn sites in SM and Co-SM. Reproduced with permission from Ref. [92], © Elsevier B.V. 2024. (e) XPS spectra of fresh and spent $Cu/Beta@CeO_2$ catalysts. Reproduced with permission from Ref. [96], © Elsevier B.V. 2023. (f) Adsorption energy of NO when toluene is pre-adsorbed. (g) Nitrogen-containing products identified by ion chromatography (IC). Reproduced with permission from Ref. [46], © Elsevier B.V. 2022. (h) Synergistic reaction mechanism of the CuCeTi catalyst. Reproduced with permission from Ref. [62], © Elsevier B.V. 2023.

redox performance and surface acidity. The presence of CB inhibited excessive NH_3 oxidation, while NO_2 generated from NO oxidation promoted deep oxidation of CB, forming a synergistic reaction pathway. Modifying surface acidity and redox properties through metal doping is another effective approach. Lin et al. [86] prepared a Fe-MnO_2-F&R composite catalyst with abundant micropores and Brønsted/Lewis acid sites (Fig. 4(c)). Fe doping increased the Mn^{4+} ratio, promoting toluene activation and NH_3 adsorption, enabling low-temperature synergistic removal. In the Co-MnO_x catalyst developed by Kang et al. [87], Co doping formed a $MnCo_2O_4$ spinel structure, enhancing Lewis acidity and promoting oxygen vacancy formation. NO_x conversion exceeded 90% within 105–275 °C, and the CB conversion reached over 90% above 180 °C. The Cu-MnO_2 catalyst prepared by Huang et al. [88] achieved 98.5% toluene conversion, although high concentrations of NO_x competed for active sites and generated nitrite intermediates, inhibiting toluene oxidation. In composite catalyst systems, the $NiMn_2O_4$-CeO_2 catalyst developed by Ma et al. [89] utilized Ni and Mn to predominantly govern NH_3-SCR and propane (C_3H_8) oxidation, respectively. NO_x conversion exceeded 80% within 100–250 °C, and the C $_3H_8$ conversion reached 90% at 210 °C. However, SO_2 readily caused sulfate deposition and deactivation. Sun et al. [90] reported an Ag-modified Mn/HZSM-5 catalyst that achieved efficient NO_x and acetone removal within 293–400 °C. The incorporation of Ag enhanced redox performance and Lewis acidity, broadening the active temperature window. Chen et al. [91] constructed a $V_{0.5}Mn_5Co_5$ bifunctional catalyst, where V doping precisely regulated acid and redox sites. While suppressing over-oxidation of ethylene, the catalyst achieved over 95% NO_x conversion and ≥ 80% N_2 selectivity within 180–300 °C, along with good resistance to sulfur and water. Zhang et al. [92] found that in a Co-doped $SmMn_2O_5$ (Co-SM) catalyst, synergistic interactions between Mn–Mn and Co–O–Mn–Mn sites enhanced redox performance and surface acidity. Co doping lowered the d-band center of Mn–Mn sites, inhibiting nitrate deposition and improving N_2 selectivity, while Co–O–Mn–Mn sites promoted deep oxidation of chlorobenzene (Fig. 4(d)). The catalyst achieved high NO_x conversion within 160–300 °C, with a T_{90} for chlorobenzene at 270 °C, N_2 selectivity > 80%, and near 100% CO_2 selectivity, demonstrating excellent synergistic catalytic performance. Ye et al. [67] prepared an MnO_x-CeO_2 catalyst supported on TiO_2 nanotubes (MnCe/TNT) for simultaneous removal of NO_x and toluene at low temperatures (≤ 300 °C). Mechanistically, the redox transitions of Mn^{3+}→Mn^{4+} and Ce^{4+}→Ce^{3+} enhanced Lewis acidity and promoted oxygen vacancy formation. This effect significantly reduced the toluene conversion temperature, suppressed side reactions such as NH_3 oxidation and N_2O formation, and ultimately enabled highly efficient simultaneous removal of NO_x and toluene while improving N_2 selectivity in the NH_3-SCR process. Additionally, the catalyst exhibited excellent hydrothermal stability and resistance to SO_2 poisoning.

In summary, strategies such as structural design, morphology control, metal doping, and composite construction can effectively enhance the catalytic performance and poisoning resistance of Mn-based catalysts for the synergistic removal of NO_x and VOCs, thereby laying a theoretical foundation and offering technical pathways for their practical application in flue gas purification.

Zeolite catalysts. Conventional zeolite catalysts exhibit significant limitations in the synergistic removal of alkanes and NO_x, primarily due to constraints imposed by their inherent crystalline structures and surface properties on reactant adsorption and catalytic activity. As typical crystalline aluminosilicates, zeolite molecular sieves hold important applications in catalysis and adsorption processes owing to their abundant acid sites and regular pore structures [93, 94]. By incorporating active components with excellent redox properties into their frameworks, bifunctional catalytic sites can be constructed, thereby synergistically promoting the efficient elimination of VOCs and NO. Chuang et al. [95] synthesized Santa Barbara Amorphous-15 (SBA-15) support via a hydrothermal method and loaded transition metals (Cu, Co, Ni), finding that Cu/SBA-15 achieved 70% toluene conversion at 250 °C. Subsequent modification with Mn yielded an Mn-Cu/SBA-15 catalyst that achieved complete toluene conversion at the same temperature; at 300 °C, it reached 70% NO removal while maintaining complete toluene conversion, demonstrating favorable synergistic catalytic performance. Jiang et al. [96] prepared a Cu/Beta@CeO_2 core–shell catalyst via a self-assembly method, systematically elucidating the roles of different active sites in the synergistic removal of NO and toluene. The study revealed competitive adsorption between NH_3 and toluene on Brønsted acid sites. The ultrathin CeO_2 layer deposited on the surface not only increased the number of Brønsted acid sites but also introduced Ce^{4+} sites that promoted toluene oxidation. Furthermore, the strong interfacial interaction at the Cu–Ce interface induced the formation of numerous Ce^{3+} and isolated Cu^{2+} sites, synergistically enhancing NH_3 activation, NO adsorption/oxidation, and their subsequent reaction with toluene (Fig. 4(e)).

Other catalysts. Beyond conventional V-based, Mn-based, and zeolite catalysts, several other catalytic systems play significant roles in the synergistic elimination of NO_x and VOCs. Based on their active components and primary mechanisms, these systems can be categorized and their synergistic pathways are discussed in greater detail.

Photocatalytic systems utilize light energy to drive reactions. For instance, Wang et al. [58] demonstrated that NO significantly enhanced the photocatalytic degradation efficiency of aromatic hydrocarbons over TiO_2. The generated NO_2 replenishes surface active oxygen, sustaining catalytic activity while promoting the conversion of NO into harmless nitrogen-containing species. The synergy primarily stems from the cross-utilization of reactive intermediates: photogenerated charge carriers (e^-/h^+) and reactive oxygen species (e.g., $\cdot O_2^-$, ·OH) couple the reduction of NO_x with the oxidation of VOCs. Li et al. [46] further revealed a mechanism of non-competitive adsorption and coupled reaction on $In(OH)_3$, where pre-adsorbed toluene enhanced NO adsorption (Fig. 4(f)), and protons/electrons released during toluene oxidation reduced NO to NH_4^+, thereby altering the reaction pathway, reducing NO_2 selectivity, and inhibiting O_3 formation (Fig. 4(g)).

CeO_2-based catalysts are widely studied due to their excellent oxygen storage capacity and reversible Ce^{3+}/Ce^{4+} redox properties. Doping strategies can finely tune their physicochemical properties. Gan et al. [59] optimized a Ce2Si1 catalyst (Ce:Si = 2:1), achieving > 90% conversion of both NO_x and toluene at 300–375 °C with high N_2 selectivity (> 95%). Li et al. [97] and Wei et al. [98] systematically studied metal-doped CeO_2; Cr doping enhanced synergistic NO_x reduction and chlorinated VOC oxidation while mitigating chlorine poisoning, whereas Al^{3+} doping increased Lewis acidity and oxygen vacancies, promoting NH_3 activation and chlorobenzene oxidation. In contrast, higher-valence Ta^{5+} doping exhibited an inhibitory

effect. Density functional theory (DFT) calculations revealed that doping modulates reaction energy barriers and oxygen vacancy formation [98]. The core synergy lies in the dynamic cycle of oxygen vacancies coupled with acid-redox site cooperation, which concurrently supplies active oxygen for VOCs oxidation and provides sites for NO_x adsorption/activation.

Dual-active-site/multifunctional catalysts employ spatially adjacent or functionally distinct sites to achieve synergistic catalysis. A Cu-Ce bimetallic catalyst achieved > 95% removal of toluene and NO at 250 °C, with Cu sites governing toluene oxidation and Ce sites facilitating NH_3-SCR. This design synergistically inhibited SO_2 adsorption and ammonium sulfate formation, enhancing sulfur resistance (Fig. 4(h)) [62]. Similarly, a CeO_2-TiO_2 mixed oxide catalyst showed excellent NH_3-SCR activity (N_2 selectivity > 96%) and, in the presence of toluene, promoted a toluene-SCR pathway, achieving 90% toluene conversion with nearly complete CO_x selectivity at 300 °C [99]. Another example is Nb-doped CeO_2, where optimal Nb doping promoted lattice oxygen migration and Lewis acidity, enabling > 90% conversion of both NO and toluene between 215 and 400 °C [100]. By regulating the position of Fe single atoms on a CoOOH substrate, Zhang et al. [101] constructed two Fe-Co dual-site catalysts with stereoscopic (stereo-Fe-Co DSC) and planar (planar-Fe-Co DSC) configurations. The planar configuration exhibited superior performance in the alkaline oxygen evolution reaction, with a significantly lower overpotential (190 mV at 10 $mA{\cdot}cm^{-2}$) than the stereoscopic analogue (210 mV). The planar Fe-Co dual sites were found to facilitate the direct coupling of $^*O$ intermediates into $^*O$–O^* species, thereby circumventing the conventional four-electron transfer pathway. The spatial distance and orientation of the dual sites directly govern the adsorption, activation, and coupling of intermediates, offering critical structural insights for the rational design of high-performance dual-site catalysts. The synergy in these systems arises from spatial proximity and functional complementarity, which mitigates competitive adsorption and allows intermediates generated at one site to promote reactions at adjacent sites.

In summary, these alternative catalysts—through light-driven charge separation, tunable redox-acid properties, or designed site cooperation—provide diverse and effective pathways for the synergistic removal of NO_x and VOCs, expanding the toolbox for multi-pollutant control.

2.3.2 *Structural optimization and modification*

In complex industrial flue gas environments, catalysts are susceptible to irreversible poisoning by alkali metals, heavy metals (e.g., As and Pb), chlorine species, and phosphorus, beyond the effects of SO_2 and H_2O. Their deactivation mechanisms differ markedly from those induced by mere sulfur or water poisoning. Alkali metals preferentially displace surface hydroxyl or Lewis acid sites, leading to a marked decline in surface acidity. This impairs NH_3 adsorption and activation, severely suppressing SCR activity, while their electronic effects alter the valence distribution and redox properties of active metals (e.g., Cu) [102, 103]. Lead primarily poisons catalysts through competitive chemisorption at active sites and alters the surface electronic structure, reducing both acidity and redox capability [104]. Its presence also shifts the chlorobenzene oxidation pathway from CB → phenol → benzoquinone → CO_2 to CB → benzene → CO_2, lowering oxidation efficiency and CO_2 selectivity. Excessive Pb further blocks pores and reduces the specific surface area [105]. Arsenic exists primarily as As_2O_3 and As_2O_5. As_2O_3 lowers the formation energy of oxygen vacancy at V–O–V sites, while As_2O_5 attacks V=O sites to form As–O–V bonds. Both mechanisms deactivate active sites and block pores, suppressing denitrification while promoting excessive NO oxidation to NO_2, which inadvertently enhances chlorobenzene conversion [106–108]. Chlorine species (e.g., Cl^- derived from CVOCs) occupy oxygen vacancies, forming inert metal chlorides/oxychlorides. They also anchor surface active oxygen, hindering O_2 adsorption and disrupting the redox cycle. Additionally, Cl^- can combine with surface NH_4^+ to form NH_4Cl, which covers active sites. The accumulation of these species further promotes the generation of polychlorinated by-products, exacerbating catalyst deactivation [109–111]. As an external poison originating from sources such as lubricating oils, phosphorus induces typically irreversible deactivation of exhaust after-treatment catalysts through a combination of physical and chemical mechanisms. Physical deactivation results from the pore blockage and surface area reduction caused by the deposition of phosphorus species. Chemical deactivation is more profound, where phosphorus in the forms of metaphosphate (PO_3^-) and phosphate (PO_4^{3-}) strongly interacts with active sites, poisoning key hydroxyl (OH) groups and forming thermally stable compounds like $AlPO_4$ via reaction with the zeolite framework. The severity of deactivation escalates with increasing phosphorus loading. Notably, during multiple adsorption–desorption cycles, a portion of physically blocking P_2O_5 transforms into chemically interacting PO_3^-, leading to progressive and irreversible degradation of the catalyst's storage and release capacity [112]. In practice, these poisons often act synergistically, severely compromising the long-term stability and efficiency of catalysts in multi-pollutant control through combined mechanisms such as pore blockage, chemisorption, electronic modulation, and alteration of reaction pathways.

To achieve efficient synergistic catalytic elimination of atmospheric pollutants, the dynamic evolution mechanisms of active sites must be considered in conjunction with stability design. Single-atom catalysts (SACs) hold potential for synergistic air purification, yet their symmetric active sites (e.g., $M–N_4$) often exhibit unbalanced adsorption toward diverse intermediates. Symmetry-breaking strategies enable the construction of asymmetric centers (e.g., $M–N_3$, $M–X–N_x$), which induce localized charge redistribution and d-band modulation to synergistically enhance adsorption of key pollutants [113]. This approach provides a foundation for designing multifunctional bimetallic sites capable of driving simultaneous NO_x reduction and VOCs oxidation, guiding the development of efficient synergistic catalytic systems. Research shows that the reversible structural transformations among single atoms, clusters, and nanoparticles can not only create functionally complementary dynamic active interfaces but also enable *in situ* regeneration and long-term stabilization of active sites through modulation of the atmosphere and support [114]. Therefore, by precisely tailoring metal–support interactions and the reaction microenvironment to steer active species toward favorable configurations and suppress deactivating agglomeration, it is possible to develop next-generation air pollution control catalysts that combine high activity with high stability.

V-based catalysts show strong stability in the presence of H_2O and SO_2 [78], but their weak redox capability often leads to incomplete VOCs oxidation and byproduct accumulation due to competitive NH_3 adsorption [79]. SO_2-derived sulfates inhibit C–C cleavage, deactivate oxygen species, and gradually poison the catalyst [89]. Mn-based catalysts offer excellent low-temperature activity but suffer from low high-temperature N_2 selectivity, a

narrow activity window, and susceptibility to sulfur poisoning [90]. Zeolite catalysts, with their structured pores, can isolate and optimize reactions for synergistic removal [96]. However, their complex synthesis and insufficient study in synergistic systems require further exploration. Future development should focus on carrier selection, synthesis methods, and active component modification to enhance overall efficiency, durability, and poisoning resistance.

(1) Carrier selection. The carrier plays a critical role in modulating catalyst performance, profoundly influencing activity, heat and mass transfer efficiency, and operational durability. In V-Cu bimetallic catalysts, the TiO_2 carrier enhances performance via strong metal–support interactions: Its unique lattice structure promotes the formation of abundant acid sites (enhancing toluene/NO_x adsorption) and oxygen vacancies (improving redox capability), outperforming conventional carriers such as ZSM-5, SiO_2, and γ-Al_2O_3. At the microscopic level, oxygen vacancies facilitate electron transfer from Cu to adsorbed O_2, generating highly reactive superoxide radicals. These directly accelerate the synergistic pathway of toluene mineralization and NO_x reduction, enabling highly efficient pollutant removal [76]. Isolated atom site catalysts (IASCs) demonstrate superior electrocatalytic activity and strong poisoning resistance in small-molecule electrooxidation reactions, owing to their atomically dispersed active centers and tunable coordination structures. By constructing dual-atom sites or support-synergistic systems, precise control over the reaction pathways can be achieved, effectively suppressing the accumulation of harmful intermediates such as CO and thereby significantly enhancing catalyst durability [52].

(2) Influence of synthesis methods. Different synthesis methods induce substantial variations in the crystal structure, surface morphology, and distribution of active sites, thereby significantly determining catalytic performance. The sol-gel method enables controlled hydrolysis–condensation to produce catalysts with high specific surface area and uniformly dispersed active sites, effectively suppressing agglomeration [87]. In contrast, co-precipitation relies on simultaneous precipitation to form precursors with well-defined crystallinity and uniform particle size [97]. Differences in crystal defect density, surface morphology, and accessibility of active sites directly govern the structure–activity relationship, necessitating careful selection based on the target reaction's kinetic characteristics.

(3) Doping modification. Doping with metal or non-metal ions represents a highly effective strategy for tailoring catalyst properties by modifying the electronic and crystal structures at the fundamental level. In Mn-Ce catalysts, metal ion doping reconstructs the electronic configuration through lattice substitution. The introduction of heterovalent ions induces charge imbalance, promoting the formation of oxygen vacancies to restore charge neutrality, thereby creating additional active sites. Concurrently, it modulates the electron density of active sites, optimizing reactant adsorption energy and reaction selectivity. Precise control over the valence state and concentration of dopants enables targeted design of the catalyst's intrinsic activity [75, 90, 98].

Beyond conventional catalyst design, drawing inspiration from interdisciplinary fields such as energy catalysis offers advanced strategic guidance for synergistic VOCs–NO_x catalytic systems. Liu et al. [115] proposed a grain-boundary engineering and dual-mechanism synergy strategy for the acidic oxygen evolution reaction (OER), providing an insightful paradigm for simultaneously boosting both catalytic activity and stability. By introducing Ni and B co-doping into RuO_2, they constructed ultrathin nanosheets rich in grain boundaries, thereby achieving spatial partitioning and synergistic enhancement between the adsorbate evolution mechanism (AEM) and the lattice oxygen mechanism (LOM) within the catalyst: Grain-boundary regions, enriched with defects and tailored electronic structures, preferentially promote the LOM pathway, while well-ordered crystal facets dominate the AEM pathway. This "spatially partitioned synergistic catalysis" design not only reduces reaction barriers through parallel dual pathways but also separately enhances interfacial activity and lattice stability via structural regulation, thereby successfully overcoming the classic activity-stability trade-off in conventional catalysts.

3 Synergistic abatement of VOCs and O_3

3.1 Synergistic abatement technologies

With the progressive industrialization in China, anthropogenic VOCs emissions continue to rise, emerging as significant precursor pollutants affecting regional air quality. As one of the key precursors to ozone formation, increasing VOCs levels exacerbate the formation and accumulation of ground-level ozone pollution, intensifying the challenges in ozone control. In this context, establishing a coordinated control system for VOCs and O_3, and advancing multi-dimensional efforts in mechanistic research, regulatory strategies, and technological innovation have become imperative to steadily advance the current air pollution mitigation agenda (Table 3).

3.1.1 Photocatalytic technology

Photocatalytic technology relies on the photoexcitation process of semiconductor materials. When incident photon energy ($h\nu$) exceeds the band gap (E_g) of the photocatalyst, electrons are excited from the valence band (VB) to the conduction band (CB), generating electron–hole pairs (e^-/h^+). The VB holes exhibit strong oxidation capability, oxidizing adsorbed H_2O or OH^- to form highly oxidative hydroxyl radicals (·OH), while CB electrons reduce adsorbed O_2 to superoxide radicals ($\cdot O_2^-$). These reactive oxygen species collectively drive the oxidative degradation and mineralization of VOCs, as illustrated in Fig. 5(a) [116, 117]. Among various photocatalysts, TiO_2 is widely utilized due to its high chemical stability, favorable photocatalytic activity, and low cost. However, its relatively wide band gap (~ 3.2 eV) restricts light absorption mainly to the ultraviolet region (only 4%–5% of solar spectrum), limiting practical efficiency under solar irradiation [118]. To address this, research has focused on modifying TiO_2 through elemental doping and heterojunction construction to narrow the band gap, extend light absorption into the visible range, and enhance charge carrier separation. Kask et al. [119] designed a multi-stage continuous-flow photocatalytic reactor to investigate the effect of O_3 on the degradation of gaseous acetone and toluene (individually and in mixtures). O_3 showed limited enhancement for acetone alone but promoted degradation of high-concentration toluene (60 ppm) and its mixtures, while mitigating catalyst deactivation caused by accumulated toluene oxidation intermediates. Humidity (6%–40%) had minimal effect on single VOCs degradation, whereas high humidity slightly suppressed degradation in VOCs mixtures. Longer residence time significantly

Table 3 Comparison of different VOCs and O_3 synergistic control technologies

Technology	Key mechanism	Typical operating conditions	Advantages	Limitations
Photocatalysis [116, 117, 120]	Generation of reactive oxygen species via photoexcited e^-/h^+ pairs to oxidize VOCs and decompose O_3.	Low VOCs concentration (< 100 ppm); sensitive to humidity (inhibited at high RH); requires UV/visible light activation	Mild operating conditions, low energy consumption, no secondary pollution; potential for solar-driven operation	Low quantum efficiency, rapid carrier recombination, catalyst deactivation, narrow light-response range.
Catalytic ozonation [44, 122, 123]	Decomposition of O_3 on catalyst surfaces to form active oxygen species for VOCs oxidation; non-radical pathways may also operate.	Low to medium VOCs concentration; humidity tolerance depends on catalyst; requires optimized O_3/VOCs ratio	Strong oxidizing capacity of O_3, fast reaction rate; catalysts improve selectivity and mineralization	Risk of by-products from excess O_3, catalyst poisoning by O_3, relatively high operational cost.
VUV–catalytic coupling [45, 124, 125]	Direct VOCs cleavage and *in-situ* O_3/·OH generation by VUV photolysis, coupled with catalytic ozonation for deep oxidation	Broad VOCs concentration range; high humidity tolerance (efficient up to ~ 65% RH); operable at room temperature	Strong synergistic effect, high mineralization efficiency, robust performance under humid and complex conditions	System complexity, high energy consumption, limited VUV lamp lifetime, potential for secondary O_3 formation

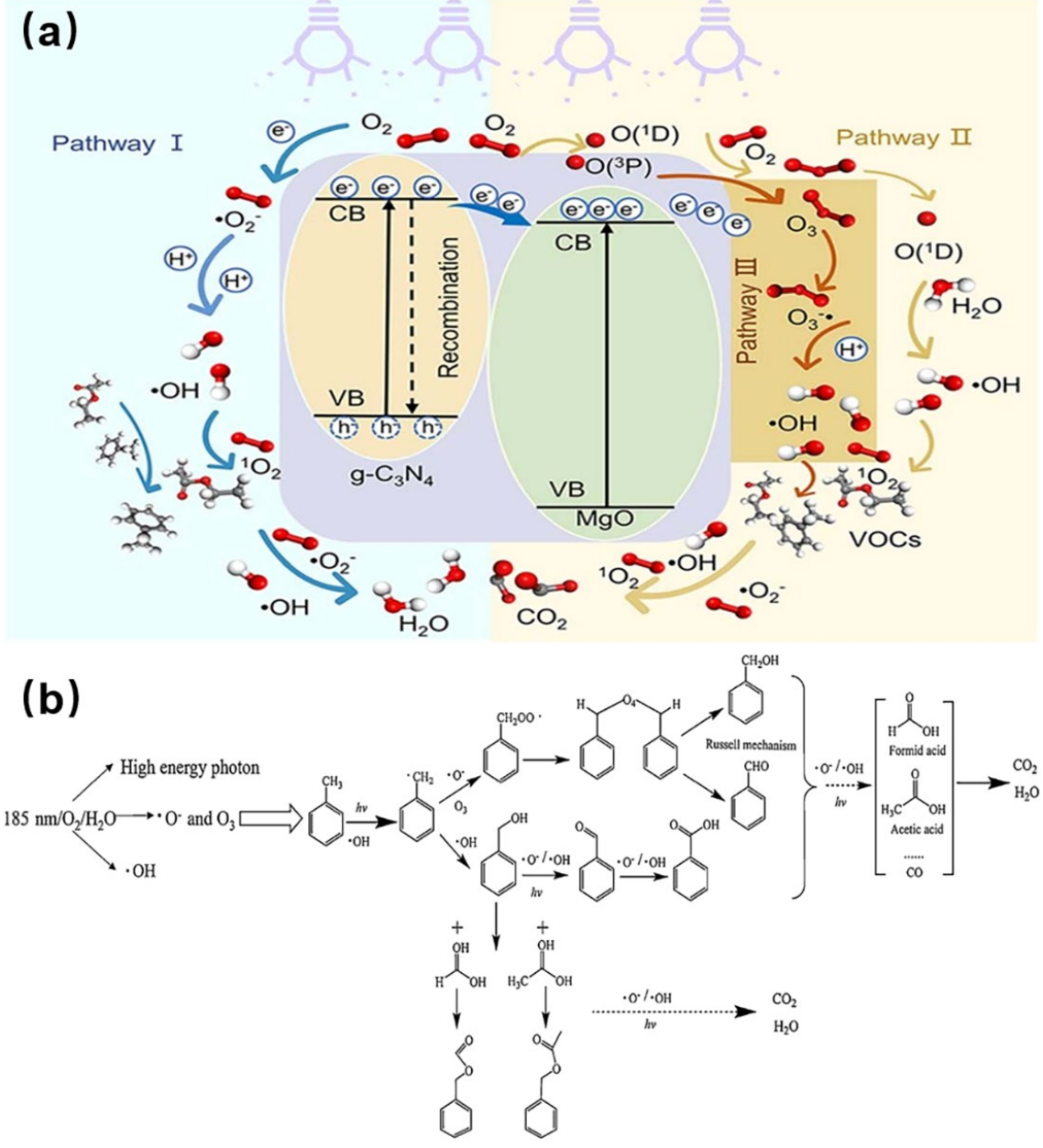

Figure 5 (a) Photocatalytic mechanism. Reproduced with permission from Ref. [120], © Sui et al. 2024. (b) Degradation pathway of toluene by VUV photolysis. Reproduced with permission from Ref. [45], © Elsevier B.V. 2018.

improved VOCs conversion. O_3 was completely decomposed over TiO_2, with higher decomposition rates under high humidity or high VOCs concentrations. The main byproducts were CO_2 and H_2O, with trace formic acid detected only under coexistence of high-content toluene and O_3. O_3 promoted CO formation, indicating a tendency toward partial oxidation. To improve photocatalytic efficiency, Dong et al. [47] integrated photocatalysis with adsorption by synthesizing a series of bimetallic metal-organic frameworks (MOFs), PCN-250(Fe_2M) (M = Co, Ni, Mn), via a solvothermal method. These were evaluated for dual-function performance in catalytic ozone decomposition and VOCs adsorption at room temperature. PCN-250(Fe_2Co) achieved 100% removal of 1 ppm O_3 across 0–80% relative humidity (Fig. 6(a)) and maintained stability for 100 h. It also exhibited high adsorption capacities (89–241 mg·g^{-1}) for ten common VOCs, even under humid conditions. Bimetallic MOFs showed superior catalytic activity to monometallic PCN-250(Fe_3), with Co(II) sites identified as key active centers. The material demonstrated excellent hydrothermal stability and ozone tolerance, maintaining structural integrity in humid air, aqueous environments, and under high O_3 exposure (50 ppm, 100 h). DFT calculations indicated lower reaction energy barriers and higher efficiency for ozone decomposition under dry conditions. Sui et al. [120] constructed MgO/g-C_3N_4 composites by pyrolyzing melamine to form g-C_3N_4, followed by MgO loading via impregnation–calcination. Under 185 nm UV irradiation, the composite simultaneously degraded VOCs (e.g., toluene and ethyl acetate) and utilized generated O_3 to produce reactive oxygen species, enabling synergistic removal of VOCs and O_3. The formation of Mg–N and C–O bonds reduced the band gap, enhancing light absorption and charge carrier separation. The material achieved > 95% toluene degradation, 75% O_3 removal, and > 85% ethyl acetate degradation, with nearly zero O_3 detected at the outlet and good cycling stability.

3.1.2 *Catalytic ozone-assisted technology*

O_3, a strong oxidant with a redox potential of 2.07 V, can partially oxidize VOCs into small molecular products [121]. However, sole reliance on O_3 often results in incomplete mineralization and by-product formation. Coupling O_3 with catalytic oxidation significantly enhances the removal efficiency to VOCs. In such systems, O_3 initially oxidizes insoluble NO into soluble NO_2, which is further converted into highly water-soluble nitric anhydride (N_2O_5), enabling synergistic multi-pollutant removal through tail-end wet scrubbing. For chlorinated VOCs like dichloromethane (DCM), the O_3-catalysis synergy effectively promotes degradation while reducing chlorinated by-products. Catalysts play a key role in enhancing reaction rate and efficiency. The system performance is influenced by factors such as the O_3/VOCs molar ratio, catalyst properties, temperature, and humidity. Notably, catalyst acidity and redox properties strongly affect reaction pathways and product distribution [122]. Ikhlaq et al. [44] systematically compared γ-Al_2O_3 and various ZSM-5 zeolites in catalytic ozonation of CVOCs.

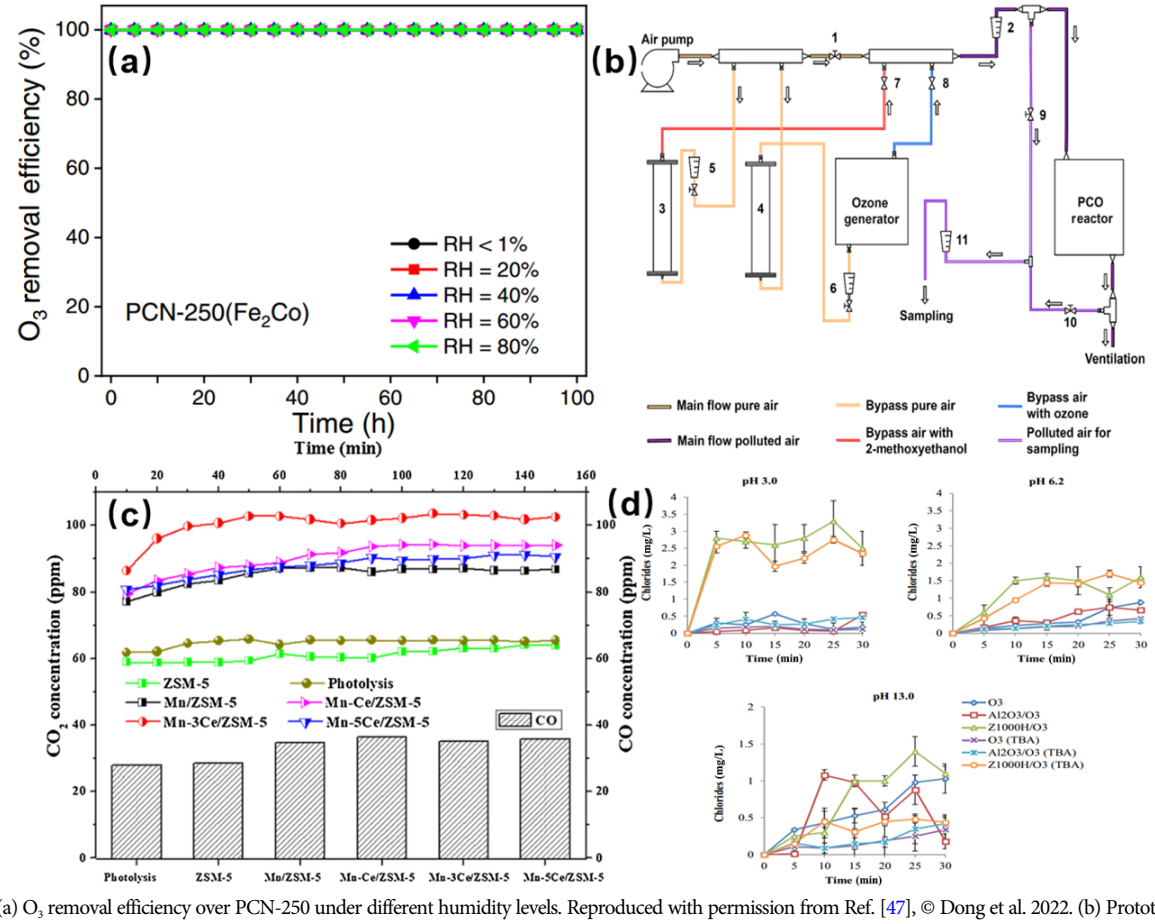

Figure 6 (a) O_3 removal efficiency over PCN-250 under different humidity levels. Reproduced with permission from Ref. [47], © Dong et al. 2022. (b) Prototype packed-bed photocatalytic reactor. Reproduced with permission from Ref. [123], © Elsevier B.V. 2024. (c) CO_x concentration of different samples in the VUV-OZCO system. Reproduced with permission from Ref. [45], © Elsevier B.V. 2018. (d) Effect of TBA on chloride formation during individual ozonation and ZSM-5 zeolite/alumina ozonation of VOCs. Reproduced with permission from Ref. [44], © Elsevier B.V. 2016.

ZSM-5 exhibited markedly higher activity, attributed to its stronger VOCs adsorption capacity. High-silica ZSM-5, with enhanced hydrophobicity, showed superior performance in adsorbing hydrophobic VOCs molecules compared to low-silica analogues (e.g., Z25H and Z25Na). Both acidic (H-form) and basic (Na-form) ZSM-5 demonstrated catalytic activity, with performance governed by the Si/Al ratio and reaction pH. Highest activity was observed under acidic conditions (pH = 3), which favor molecular ozone stabilization and catalyst surface adsorption. To overcome inherent limitations of photocatalysis, Altof et al. [123] integrated O_3 into a photocatalytic process using a 21.3 L prototype packed-bed photocatalytic (PCO) reactor (Fig. 6(b)) for simultaneous treatment of 2-methoxyethanol (2ME) and O_3 at room temperature. A synergistic effect was observed in the co-presence of 2ME and O_3: 2ME degradation increased from 5 ppm to 9.5 ppm, the O_3 degradation reached 95%, and the reaction kinetics shifted from pseudo-zero-order to second-order. Major by-products included formic acid, methyl formate, and formaldehyde (the latter only formed when O_3 was present). The PCO reactor is suitable for low concentrations (< 10 ppm) and long residence time (77 s), and can be combined with pulsed corona discharge (PCD) technology for treating higher VOCs concentrations.

3.1.3 *Other synergistic technologies*

Beyond photocatalysis and ozone-assisted technologies, synergistic techniques such as vacuum ultraviolet (VUV) photolysis (Fig. 5(b)) combined with catalytic ozonation, as well as thermal catalysis, have also been applied for the co-removal of VOCs and O_3. In VUV processes, high-energy photons (100–200 nm) directly cleave chemical bonds (e.g., C–C and C–H) in VOCs molecules, generating radicals and small molecular products [124, 125]. To address challenges in conventional catalytic ozonation, such as catalyst deactivation, humidity inhibition, and secondary pollution at room temperature, Payan et al. [126] proposed an integrated system coupling a VUV reactor with a fixed-bed catalytic ozonation reactor. Using 185 nm VUV as an ozone source, along with reactive species (e.g., O_3 and ·OH) and an Ag/CeO_2-Al_2O_3 catalyst, the system achieved efficient deep oxidation of VOCs. Compared to individual systems, the coupled setup increased the conversion of acetone and ozone from ~ 82% and 86% to 100%, maintaining complete conversion even at 65% relative humidity. Al_2O_3 promoted acetone adsorption and ozone conversion, while CeO_2 enhanced CO oxidation toward complete mineralization. With a CeO_2:Al_2O_3 ratio of 1:1, the Ag/CeO_2-Al_2O_3 (AgCeA) catalyst achieved full acetone conversion, complete ozone decomposition, and 99% mineralization selectivity at room temperature. The team further evaluated α-MnO_2-based catalysts in the coupled system [127]. Pure α-MnO_2, α-MnO_2/TiO_2, and α-MnO_2/γ-Al_2O_3 all achieved complete conversion of acetone and ozone in the integrated setup, far outperforming single systems. Although humidity inhibited the fixed-bed catalyst activity, it enhanced the VUV process, allowing the system to remain effective up to relative humidity (RH) ≤ 65%. The highest CO_2 yield (431 ppm) was observed in the coupled system, with no CO or harmful intermediates detected, indicating a shift toward complete oxidation. Shu et al. [45] synthesized a series of Mn-*x*Ce/ZSM-5 catalysts (Fig. 6(c)) via impregnation for a VUV-catalytic ozonation system to synergistically degrade toluene and remove byproduct ozone. The optimal catalyst achieved 93% toluene degradation and nearly 100% O_3 removal, with a mineralization rate 1.2 times higher (54%) than that of VUV alone. Ce doping formed Mn–O–Ce bonds, enhancing redox properties, increasing the Ce^{3+} ratio and oxygen vacancy density, thereby promoting ozone adsorption and activation. Wang et al. [128] designed a core–shell C@MnO trifunctional catalyst for simultaneous removal of HCHO and ozone at room temperature. The carbon core adsorbs and enriches HCHO, while the MnO shell catalyzes ozone decomposition and oxidizes HCHO, effectively preventing etching of the carbon material in an ozone-rich environment. The catalyst achieved 100% removal of HCHO and O_3, 100% CO_2 selectivity, and long-term stability, offering a high-performance material for indoor air purification and plasma/electrostatic exhaust treatment (Table 4).

3.2 Synergistic mechanisms

The reaction mechanism between O_3 and VOCs involves multiple reactive intermediates and elementary steps, holding significant implications for both atmospheric chemistry and pollution control. Due to its unique electronic structure, O_3 readily undergoes addition reactions with unsaturated VOCs containing C=C or C≡C bonds, representing a primary pathway for its interaction with olefinic VOCs [125]. In VUV photolysis, high-energy photons not only directly dissociate VOCs molecules but also generate active sites on catalyst surfaces, facilitating subsequent reactions. In catalytic ozonation, O_3 decomposes on catalysts (e.g., Mn-Ce/ZSM-5), yielding highly reactive species such as ·OH and $\cdot O_2^-$, which progressively oxidize VOCs to CO_2 and H_2O. Under synergistic VUV–catalytic ozonation, photolytically generated radical fragments are more readily further oxidized by catalytic active species, establishing a mutually reinforcing reaction cycle that significantly enhances VOCs degradation efficiency. A study [44] on catalytic ozonation of chlorinated VOCs over γ-Al_2O_3 and ZSM-5 zeolites showed that adding the radical scavenger tert-butanol (TBA) had negligible impact on VOCs degradation rate and chlorinated byproduct formation in ZSM-5 systems, whereas a

Table 4 VOCs-O_3 synergistic performance summary

Catalyst [Ref.]	Preparation method	VOCs conversion efficiency (%)	O_3 conversion efficiency (%)	Selectivity (%)	Reaction type
Ag-CeO_2-Al_2O_3 [126]	Impregnation method	100	100	99	VUV–ozonation
P25-TiO_2 [119]	—	100	100	~ 100	Photocatalysis
C-$Mn_{0.6}$-550 [128]	Two-step method	100	100	100	Thermocatalysis
PCN-250(Fe_2Co) [47]	—	> 93	100	—	Photocatalysis Integrated with adsorption
MgO/g-C_3N_4 [120]	Impregnation-calcination method	> 95	~ 75	—	Photocatalysis
Mn-xCe/ZSM-5 [45]	Impregnation method	93	100	54	VUV–ozonation
α-MnO_2/TiO_2/γ-Al_2O_3 [127]	Hydrothermal method	100	100	—	VUV–ozonation

slight suppression of chloride generation was observed in the Al_2O_3 system, suggesting limited radical involvement in its less efficient pathway. This indicates that ZSM-5 primarily follows a non-radical mechanism, where adsorbed VOCs react directly with molecular ozone (Fig. 6(d)). Higher chloride ion concentrations detected in ZSM-5 systems confirm effective C–Cl cleavage, promoting deep oxidation and mineralization. VOCs degradation in all systems followed pseudo-first-order kinetics. Additionally, Ma et al. [129] combined field observations with a box model and found that chlorine radicals significantly promoted VOCs oxidation, increasing the net ozone production rate by approximately 0.61 ppb·h^{-1} when chlorine chemistry was considered. Chlorine radicals enhance ozone formation by promoting HO_2 and RO_2 generation, while also facilitating the formation of SOA precursors (OOMs). OOM production was sensitive to VOCs/NO_x ratios, with chlorine chemistry playing a more pronounced role under polluted conditions. This study provides the first systematic quantification of chlorine chemistry's contribution to VOCs consumption and O_3/SOA formation, offering new perspectives for synergistic pollutant control.

4 Synergistic abatement of multi-component VOCs

4.1 Synergistic abatement technologies

VOCs exhibit considerable diversity in chemical structure and originate from a wide range of sources, leading to the common occurrence of complex multi-component VOCs mixtures in ambient environments. To address such mixed VOCs pollution, a variety of control technologies have been developed. These include widely applied methods such as photocatalysis, thermal catalysis, and photothermal synergistic catalysis, as well as other approaches like adsorption separation using selective adsorbents and biological treatment based on microbial degradation. Given the significant differences among these technologies in terms of applicable VOCs types (e.g., polar/non-polar, readily/recalcitrant degradable), effective concentration ranges (high/low), removal efficiency, operational cost, and environmental adaptability, targeted selection and optimization are essential in practical applications. This ensures efficient removal of atmospheric VOCs, mitigates their potential risks to air quality and human health, and supports regional air pollution control and green ecological development.

Adsorption technology utilizes porous materials to capture VOCs from waste streams via physical or chemical interactions, achieving efficient purification. Its performance primarily depends on the pore structure and surface properties of adsorbents—such as activated carbon, activated carbon fibers, zeolite molecular sieves, and MOFs—which immobilize VOCs molecules on their surfaces [130]. Activated carbon, characterized by its high specific surface area and developed pore structure, enables rapid VOCs adsorption and surface enrichment. It is suitable for multi-component, low- to medium-concentration VOCs systems at room temperature, particularly when N_2 is used as the carrier gas [131, 132]. Activated carbon fibers (ACFs) offer larger specific surface areas and pore volumes than granular activated carbon, making them more effective under low-concentration, high-flow-rate conditions [133]. Zeolite molecular sieves feature tunable surface areas and channel structures, and exhibit advantages over activated carbon in terms of hydrophobicity and non-flammability. However, their synthesis involves multiple steps—including crystallization, ammonium exchange, washing, hydrothermal treatment, and calcination—resulting in a complex, time-consuming process accompanied by waste emissions. Furthermore, certain zeolites rely on costly raw materials (e.g., tetraethyl orthosilicate, tetraethylammonium hydroxide, and cetyltrimethylammonium bromide), leading to high production costs. Thus, developing low-cost, streamlined, and environmentally friendly synthesis routes represents a key future research direction for zeolites [134]. MOFs exhibit exceptional performance in adsorbing multicomponent VOCs due to their high specific surface area, tunable pore structures, and modifiable surface chemistry. The microstructural characteristics of MOFs are closely linked to their nucleation and growth mechanisms. Using *in situ* liquid-phase and cryogenic transmission electron microscopy, Liu et al. [135] revealed that the nucleation of zeolitic imidazolate framework-8 (ZIF-8) followed a three-step mechanism: liquid–liquid phase separation of the precursor solution into solvent-rich and solvent-lean regions; condensation of the solvent-rich regions into amorphous aggregates; subsequent crystallization of these aggregates into crystalline MOFs. This nonclassical nucleation pathway demonstrates that MOFs can develop rich mesostructures through phase separation and condensation during early formation stages, thus influencing their final pore distribution, crystal morphology, and surface active sites. Understanding MOF nucleation mechanisms aids in the rational design of MOFs with tailored porosity and surface properties, thereby optimizing their adsorption selectivity and capacity for complex VOCs mixtures and providing theoretical guidance for developing high-performance adsorbents. Modifying the organic linkers within MOFs frameworks can further enhance their hydrophobicity and adsorption selectivity [136, 137]. Studies indicate that hierarchical porosity developed at high temperatures facilitates the diffusion of aromatic VOCs, while non-covalent interactions between methyl groups and carbonized MOFs derivatives strengthen adsorption affinity. For aromatic compounds, the degree of hierarchical porosity is a critical factor governing adsorption performance. In contrast, for small oxygen-free VOCs, adsorption is predominantly physical and exhibits weaker affinity (Fig. 7(a)) [138].

Electrocatalytic systems integrating anodic oxidation of VOCs with cathodic CO_2 reduction represent an emerging strategy for simultaneous pollutant removal and chemical valorization. Zhang et al. [139] reported a $Bi_{1,n}$-pBi_2O_{3-x} catalyst that achieved efficient CO_2-to-formate conversion, coupled with methanol oxidation over a CuO_x/$ZnCo(OH)_4$ anode. In a flow-cell electrolyzer, this system attained a formate production rate of 4980 μmol·h^{-1}·cm^{-2} at 200 mA·cm^{-2}, with Faradaic efficiencies exceeding 90% at both electrodes. This approach not only degrades methanol—a representative VOCs, but also converts CO_2 into value-added formate, illustrating a dual-functional pathway for synergistic pollution control and carbon utilization. Electrocatalytic H_2O_2 production via atomically dispersed catalysts allows green *in-situ* oxidant supply. Coupled with the Electro-Fenton process through precisely engineered active sites, it drives synergistic oxidation, delivering an innovative atomic-to-process solution for the cooperative deep treatment of atmospheric pollutants [140].

Biological treatment technology utilizes microbial metabolism to degrade VOCs, converting them into harmless inorganic products (e.g., CO_2 and H_2O) and cellular constituents [142]. In this process, pollutants from the waste gas first dissolve or adsorb into the liquid

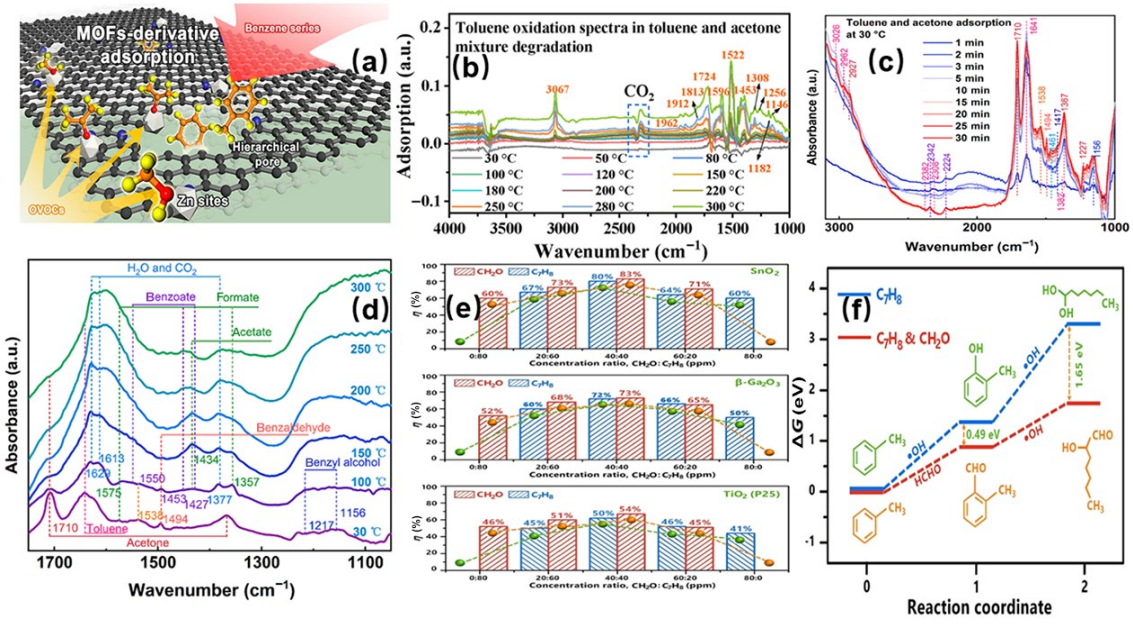

Figure 7 (a) Adsorption mechanism. Reproduced with permission from Ref. [138], © American Chemical Society 2023. (b) Extracted toluene signal from the degradation of toluene and acetone mixture over Pd/ZrO_2 catalyst. Reproduced with permission from Ref. [49], © American Chemical Society 2024. (c) *In situ* DRIFTS spectra of toluene/acetone mixture adsorption on CuC@NaY-3. (d) *In situ* DRIFTS spectra of catalytic oxidation for toluene/acetone mixture over CuC@NaY-3. Reproduced with permission from Ref. [50], © Elsevier B.V. 2024. (e) Photocatalytic efficiency evaluation of the mixture over SnO_2. (f) Changes in Gibbs free energy before and after formaldehyde addition. Reproduced with permission from Ref. [141], © American Chemical Society 2020.

phase and diffuse across the gas film into the liquid film. They then penetrate the biofilm driven by concentration gradients or microbial uptake, ultimately being captured and utilized by microorganisms as substrates for growth and metabolism. Currently, mainstream biological technologies include bioscrubbing, biofiltration, and biotrickling filtration [143]. These methods are suitable for treating low-concentration, biodegradable VOCs, commonly applied in wastewater treatment plants, landfills, and food processing industries. Advantages include low operating costs, minimal energy consumption, no need for chemical additives, and absence of secondary pollution. Compared to physicochemical methods, biological systems offer stable long-term operation and lower maintenance requirements. However, biological treatment exhibits limited efficacy for high-concentration or recalcitrant organics, with relatively low microbial degradation rates and long reaction cycles. Treatment performance is also highly dependent on environmental parameters such as temperature, humidity, and pH, requiring precise operational control and thus introducing practical complexities [144]. Recent advances in genetically engineered strains, innovative reactor designs such as modular bio-trickling filters, and hybrid multi-technology systems have significantly enhanced VOCs degradation efficiency and expanded application potential, providing key technological support for green VOCs treatment [145].

4.2 Synergistic mechanisms

The composition and interactions of VOCs significantly influence their synergistic control efficiency. The adsorption–reaction behavior of VOCs is governed by molecular structure, polarity, and the resulting surface interactions. Simple non-polar molecules interact weakly with catalysts, while those containing polar functional groups preferentially occupy active sites through stronger interactions, leading to competitive adsorption and inhibiting the conversion of other components [134]. During the catalytic degradation of multi-component VOCs, complex interactions often arise among different constituents, which can be either mutually promotional or inhibitory. The specific effects depend on factors such as VOCs types, composition, and catalyst properties. Bi et al. [49] demonstrated that in the co-degradation of toluene and acetone, acetone competitively adsorbed and inhibited both the adsorption and oxidation of toluene, particularly impeding its ring-opening to maleic anhydride (Fig. 7(b)). Conversely, toluene suppresses the polymerization of acetone to isophorone, thereby freeing active sites and enhancing acetone oxidation. Liu et al. [50] further revealed that in toluene/acetone mixtures, oxygenated intermediates (e.g., enol functional groups) generated from acetone oxidation acted as Lewis bases, promoting toluene oxidation and significantly reducing its apparent activation energy and T_{90} (Figs. 7(c) and 7(d)). In a photocatalytic study on the degradation of formaldehyde and toluene mixtures, Li et al. [141] observed that introducing formaldehyde markedly enhanced toluene degradation (Fig. 7(e)), particularly facilitating aromatic ring cleavage by significantly lowering the Gibbs free energy of ring opening. This process promoted the formation of key intermediates such as Enol Functional Group, enhancing aromatic ring adsorption and activation (Fig. 7(f)). He et al. [48] reported a synergistic promotion in the co-oxidation of acetone, ethyl acetate, and toluene over a Mn-based catalyst, where the mixture exhibited significantly higher oxidation efficiency than individual components, with notably improved toluene conversion. The study first revealed that acetone and ethyl acetate generated o-/m-cresol during toluene combustion, altering the rate-determining step of ring opening and thereby enhancing low-temperature toluene conversion (Figs. 8(a) and 8(b)). Tian et al. [146] investigated competitive adsorption and synergistic reactions of sulfur-containing VOCs (CH_3SH and C_2H_5SH) over a La/ZSM-5 catalyst: C_2H_5SH adsorbed more readily at low temperatures, while CH_3SH dominated at elevated temperatures. The addition of CH_3SH considerably reduced the

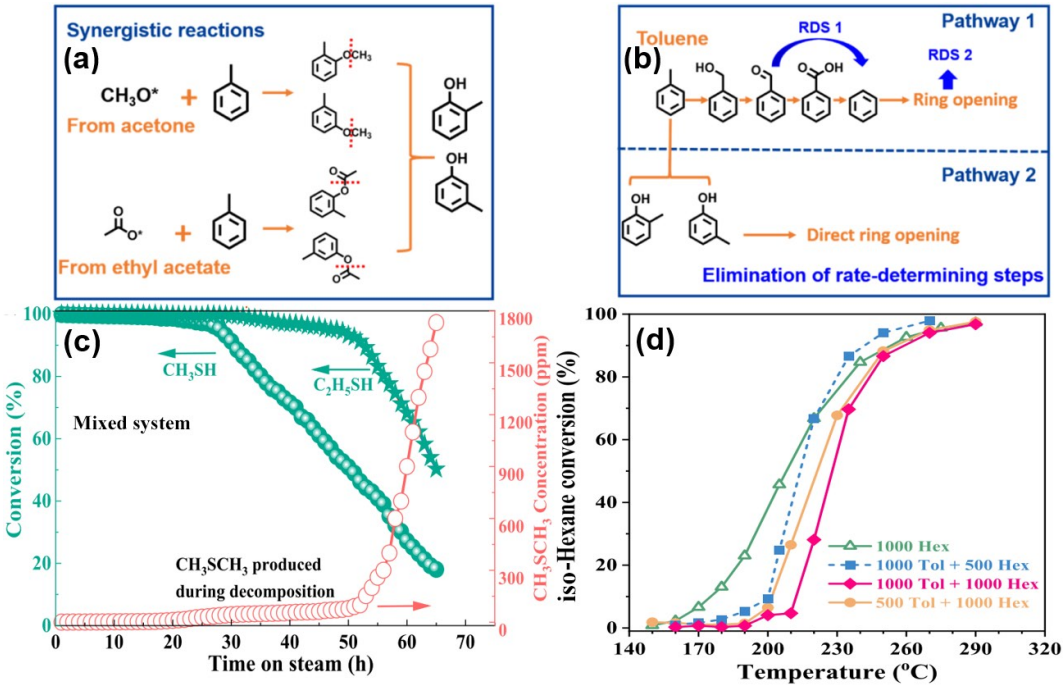

Figure 8 Proposed catalytic mechanism for complete oxidation via (a) synergistic reactions in the VOCs mixture and (b) the toluene oxidation pathway over the MnO_2 catalyst. Reproduced with permission from Ref. [48], © American Chemical Society 2022. (c) Stability profiles (green plots) and concentration of CH_3SCH_3 (red plots) formed from decomposition of CH_3SH (green spheres) and C_2H_5SH (green pentagrams) in the dual-component system. Reproduced with permission from Ref. [146], © American Chemical Society 2022. (d) Degradation rate of isohexane under different reaction conditions. Reproduced with permission from Ref. [148], © Elsevier B.V. 2023.

600 h stability originally observed for C_2H_5SH in single-component systems (Fig. 8(c)). Gao et al. [147] noted that trichloroethylene (TCE) had limited impact on o-xylene degradation, with its partial catalyst deactivation being reversible, while the presence of aromatic hydrocarbons significantly suppressed the adsorption strength of TCE, resulting in excellent catalytic stability during mixed VOCs oxidation. Feng et al. [148] further found that at lower temperatures, toluene inhibited the oxidation of isohexane, with the inhibition intensifying as toluene concentration increased; this inhibitory effect gradually diminished at higher temperatures (Fig. 8(d)).

4.3 Catalysts for multi-component VOCs synergistic abatement

Unlike the treatment of binary systems like VOCs-NO_x or VOCs-O_3, the synergistic control of multicomponent VOCs faces the core challenge of interwoven reaction networks: Molecules with different polarities, reactivities, and adsorption strengths compete for active sites and interfere with each other's reaction pathways on the catalyst surface. This necessitates a shift in catalyst design—from merely optimizing activity toward one or two pollutants—to constructing active interfaces that can selectively activate, sequentially convert, or spatially separate multiple reactants. Accordingly, the evaluation criteria extend beyond single-component conversion efficiency to include overall conversion of all components, the ignition temperature (T_{90}) of key refractory species, and selectivity toward suppressing toxic intermediates, especially those formed via cross-reactions.

4.3.1 Noble metal catalysts

Noble metal catalysts (e.g., Pt, Pd, and Ru) demonstrate advantages in treating complex mixtures containing refractory components (such as aromatics and chlorinated VOCs) due to their high activity. However, in multicomponent environments, their design requires special attention to mitigating activity suppression caused by competitive adsorption and resisting synergistic poisoning from multiple impurities (e.g., Cl, and S). Pt-based catalysts exhibit exceptional activity for the low-temperature oxidation of aromatic hydrocarbons, effectively converting them into harmless products. Tian et al. [146] investigated La-modified ZSM-5 (13% La loading via impregnation) for synergistic reactions and deactivation mechanisms during the catalytic degradation of dimethyl sulfide (CH_3SH) and ethyl mercaptan (C_2H_5SH) mixtures. La/ZSM-5 demonstrated good stability and water resistance under low concentrations and high steam conditions, indicating practical application potential. For systems containing both chlorinated and non-chlorinated VOCs, preventing the poisoning of noble metal active sites by chlorine species is crucial. Dai et al. [147] designed Pt-based catalysts using a site isolation strategy, supporting Pt, Pt_3Sn, and Pt_3Sn(E) nanoparticles on commercial CeO_2. The Pt_3Sn(E)/CeO_2 bimetallic catalyst exhibited excellent chlorine resistance in the co-oxidation of o-xylene and TCE (Fig. 9(a)). The introduction of Sn not only modulates the electronic structure of Pt but also, through adjacent Sn–O acidic sites, promotes C–Cl bond cleavage and HCl release, thereby protecting the oxidation activity of Pt sites. This targeted construction of dechlorination centers constitutes a unique strategy specific to the deactivation modes in multicomponent chlorine-containing systems. Further, Wang et al. [149] loaded Pt particles with different morphologies onto CeO_2 and evaluated their performance for toluene and chlorobenzene oxidation under pure oxygen and ozone. The superior performance of Pt/CeO_2 was attributed to the strong metal–support interaction between Pt and CeO_2, thereby increasing oxygen vacancy

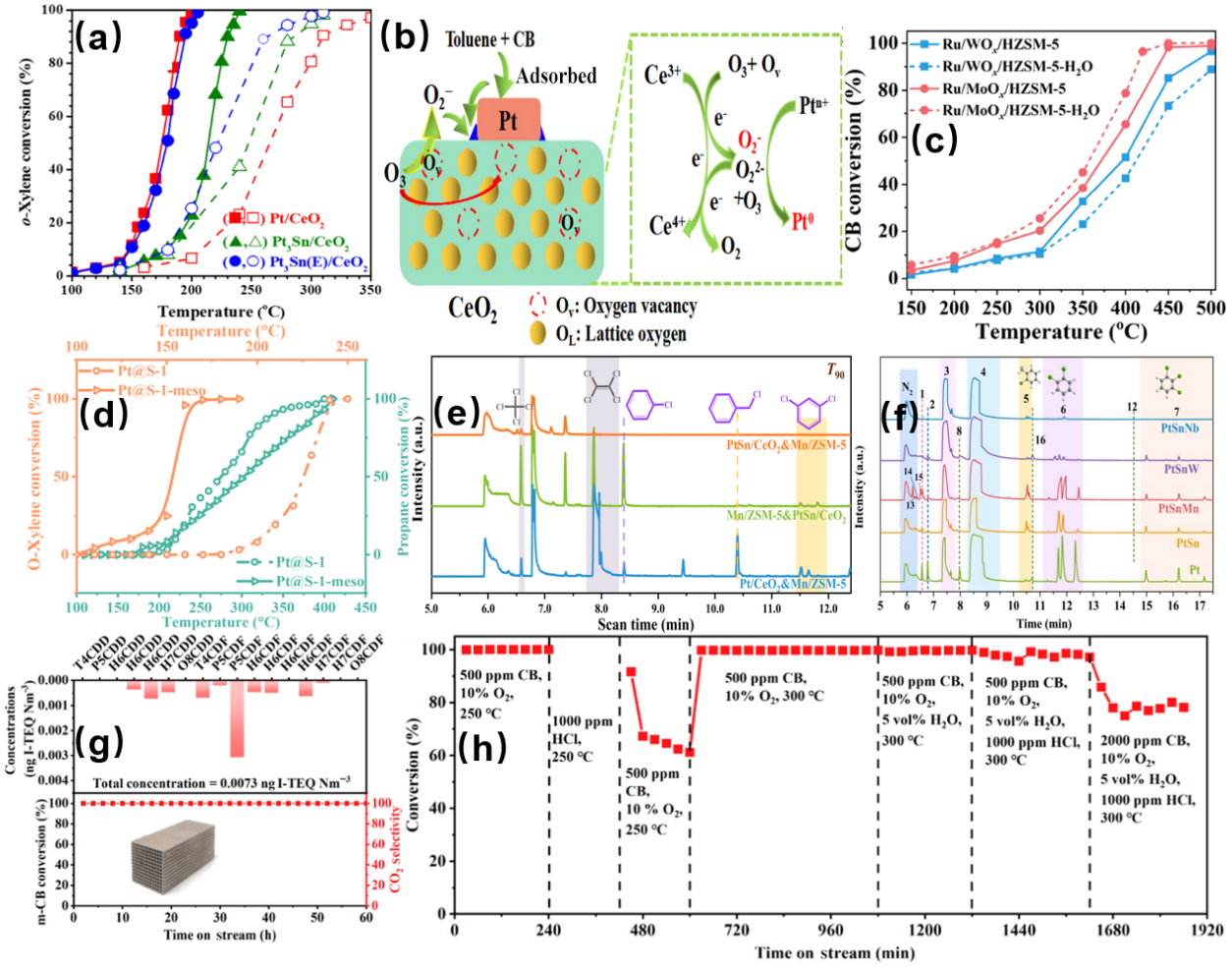

Figure 9 (a) o-Xylene conversion over the samples as a function of temperature in the absence (solid curves) and presence (dashed curves) of 100 ppm TCE. Reproduced with permission from Ref. [147], © American Chemical Society 2022. (b) Proposed mechanism for toluene and chlorobenzene oxidation over the Pt NRs/CeO_2 sample. Reproduced with permission from Ref. [149], © American Chemical Society 2023. (c) Chlorobenzene conversion over the samples in mixed VOCs oxidation. Reproduced with permission from Ref. [150], © American Chemical Society 2025. (d) Catalytic activity of Pt@S-1-meso and related catalysts for complete oxidation of the binary mixture. Reproduced with permission from Ref. [151], © Elsevier B.V. 2024. (e) Qualitative analysis of gaseous byproducts generated by the obtained samples at the temperature corresponding to 90% TCE conversion. Reproduced with permission from Ref. [152], © Elsevier B.V. 2023. (f) Qualitative analysis of gaseous byproducts generated by different samples in the presence of 5 vol% steam water. Reproduced with permission from Ref. [153], © Elsevier B.V. 2023. (g) Durability, CO_2 selectivity, and concentration of 17 toxic dioxins in the exhaust gas during m-chlorobenzene oxidation over the Ru/SnCe catalyst at 300 °C. (h) H_2O and HCl resistance during m-chlorobenzene oxidation over Ru/SnCe. Reproduced with permission from Ref. [154], © American Chemical Society 2022.

concentration, promoting ozone decomposition, and facilitating reactive oxygen species generation (Fig. 9(b)).

Additionally, Wu et al. [150] reported that the Ru/MoO_x/HZSM-5 catalyst demonstrated excellent performance for the oxidation of chlorobenzene and ethyl acetate (EA) under both dry and humid conditions, with notably enhanced activity under humidity (Fig. 9(c)). The catalyst increased the number of structural hydroxyl groups and balanced surface acidity, significantly improving catalytic stability. Water vapor introduction promoted H_2O activation, forming bridging hydroxyl groups that provided a proton-rich environment conducive to hydrolytic oxidation. This accelerated C–Cl bond cleavage and EA hydrolysis, effectively suppressing the formation of chlorinated byproducts. Feng et al. [155] synthesized a single-atom platinum catalyst supported on manganese oxide (Pt_1/MnO_x) via a molten salt method and evaluated its performance in the catalytic oxidation of toluene and isohexane-typical emissions from furniture coating industries. While Pt_1/MnO_x showed poor stability in toluene oxidation but higher stability in isohexane oxidation, its toluene oxidation stability significantly improved following H_2 pretreatment. The treated catalyst exhibited weaker Mn–O bonds, lower Pt–O coordination numbers, enhanced lattice oxygen mobility, and appropriate toluene adsorption capacity. However, its application is constrained by high cost and susceptibility to chlorine poisoning. He et al. [151] introduced mesopores into silicalite-1 to prepare Pt@S-1-meso, which demonstrated excellent activity in o-xylene oxidation (Fig. 9(d)). This diffusion-enhancing effect persisted even in the presence of smaller propane molecules. The silanol nests in the catalyst effectively enriched o-xylene near Pt nanoparticles and participated in the reaction pathway, promoting catalytic degradation. To fundamentally avoid detrimental competition between VOCs of different properties on a single active site, the concepts of tandem catalysis or functional zoning are widely employed. Li et al. [152] designed a novel tandem catalyst, PtSn/CeO_2-Mn/ZSM-5, for multi-VOCs oxidation. The catalyst comprises two independent components: PtSn/CeO_2 for oxidizing

toluene to CO_2 and H_2O, and Mn/ZSM-5 for deep oxidation of TCE. The tandem system achieved high efficiency with T_{90} values of 296 °C for toluene and 384 °C for TCE, while generating minimal toxic byproducts such as chlorobenzene and 4-chlorotoluene (Fig. 9(e)). It also exhibited excellent chlorine and water tolerance. Gao et al. [153] investigated ternary PtSnM/CeO_2 catalysts (M = Mn, W, Nb) for toluene and chlorobenzene oxidation. These catalysts demonstrated superior activity and chlorination resistance through closely coupled multi-active sites, effectively suppressing the formation of toxic chlorinated byproducts (Fig. 9(f)). Long et al. [154] developed a Ru-modified SnO_2/CeO_2 composite oxide catalyst for multi-VOCs oxidation. By controlling Ru selective adsorption on SnO_2 and CeO_2, they rationally tailored the catalyst's oxidation and dechlorination centers: Ru on SnO_2 enhanced dechlorination capability, while Ru on CeO_2 served as the oxidation center, activating H_2O to supply protons for HCl formation (Fig. 9(g)). The resulting Ru/SnO_2/CeO_2 catalyst exhibited stable performance at 300 °C for various VOCs, including chlorinated and conventional compounds (Fig. 9(h)). This spatial segregation of functions effectively mitigates cross-interference between reactants and intermediates on a single active phase and represents an advanced design strategy that directly addresses the complexity of multicomponent reaction networks.

4.3.2 *Transition metal oxide catalysts*

Transition metal oxide catalysts (e.g., MnO_2, CeO_2, and Co_3O_4) are relatively low-cost, yet their application in multicomponent systems must address the challenge that a single redox property is often inadequate to match diverse VOCs molecules. Therefore, research focuses on fine-tuning the surface acidity, oxygen vacancy density, and lattice oxygen mobility of the catalyst through strategies such as doping and compositing, aiming to create a "multifunctional" surface capable of simultaneously accommodating multiple reaction pathways. Modification of MnO_x-based catalysts aims to expand their oxidative universality. Pan et al. [48] investigated the catalytic oxidation of typical industrial VOCs mixtures (acetone, ethyl acetate, and toluene) over manganese-based catalysts (MnO_2, Mn_2O_3, $LaMnO_3$, and Mn_3O_4). It revealed for the first time a novel cross-promotion mechanism within the multicomponent system: in the co-oxidation of acetone, ethyl acetate, and toluene, the presence of acetone and ethyl acetate alters the ring-opening pathway of toluene, significantly lowers the apparent activation energy for its conversion by generating o-/m-cresol intermediates. This suggests that multicomponent catalysis may extend beyond mere competition to achieve positive synergy. Gao et al. [156] developed Ce-doped α-MnO_2 (MnCe) catalysts, and Ce incorporation regulated oxygen vacancies and acid sites. The MnCe-7% catalyst exhibited outstanding multi-VOCs oxidation performance, excellent low-temperature activity, and long-term stability, maintaining high efficiency even under humid conditions. Ce doping significantly increased oxygen vacancy concentration and acid site density, facilitating VOCs adsorption and oxidation. The superior oxygen storage capacity of CeO_2-based catalysts buffers fluctuations in dynamic feed compositions. Introduction of aliovalent dopants enables precise tuning of Lewis acidity and the kinetics of active oxygen species, thereby directing the preferential adsorption and activation order of different VOCs. Ultimately, such regulation optimizes the reaction pathway for the most recalcitrant components in the mixture, enhancing the overall mineralization depth. Xie et al. [157] achieved efficient degradation of aromatic VOCs mixtures (chlorobenzene, styrene, and toluene) in a MoS_2-enhanced Fe^{3+}/peroxymonosulfate (PMS) reaction system. The MoS_2-Fe^{3+}/PMS system deeply oxidized mixed AVOCs to CO_2 and H_2O. Differences in molecular structure, adsorption behavior, and ring-opening pathways on MoS_2(001) surfaces led to varying degradation efficiencies. Reactive oxygen species generated from PMS and O_2 activation exhibited synergistic effects, with molecular oxygen significantly shortening degradation pathways and reducing toxic intermediates. This study provides an efficient strategy for simultaneous removal of multiple gaseous AVOCs, advancing the practical application of wet scrubbing-assisted advanced oxidation processes (WSAOPs) for hazardous waste gas treatment.

4.3.3 *Other types of catalysts*

To address the differences in physicochemical properties among multicomponent VOCs, developing support materials with shape-selective or combined adsorption–catalysis functionality is a key research direction. Liu et al. [50] fabricated a CuC@NaY composite catalyst via zeolite-induced defect engineering. By integrating the high specific surface area of porous carbon with the shape-selective adsorption properties of the zeolite, this material enables the preconcentration and sieving of molecules with different polarities (e.g., toluene and acetone). This mitigates their direct competition for active sites and results in high CO_2 selectivity during the oxidation of mixtures, illustrating the design concept of synergistic adsorption-enrichment and catalytic conversion for multicomponent control. Dong et al. [141] synthesized SnO_2 via a hydrothermal method and evaluated its performance in degrading formaldehyde and toluene individually and in mixtures. The degradation efficiency for the mixture significantly surpassed that of single components, reaching 80% for HCHO and 83% for toluene at a 40:40 ppm mixing ratio. The SnO_2 photocatalyst maintained stable performance over 8 h of continuous illumination and exhibited only minor efficiency loss after 30 d of air exposure, demonstrating good stability. Furthermore, An et al. [158] derived a $ZnCoO_x$ catalyst from the pyrolysis of a bimetallic ZnCo-MOF precursor. This catalyst inherits the uniformly distributed active sites and hierarchical porous structure of the precursor, demonstrating excellent and stable elimination performance toward typical VOCs mixtures (e.g., benzene, toluene, and cyclohexane). This highlights precursor engineering as an effective route for constructing catalysts capable of adapting to complex compositions. High-entropy oxides (HEOs), as an emerging class of multi-component solid solutions, show considerable potential in complex catalytic systems due to their configurational entropy, tunable electronic structures, and stability. Recent studies have further enhanced their performance through morphological engineering. Lei et al. [159] employed a coordination-etching templating method to successfully synthesize a library of spinel-structured HEO hollow nanocubes ranging from ternary to octonary compositions. This approach achieves a uniformly distributed hollow architecture with multiple elements at low temperatures by balancing co-precipitation and etching kinetics. The resulting quinary NiCoFeCdCr-O hollow nanocubes exhibit a high reaction rate (1.79 min^{-1}) and good cycling stability (> 10 cycles) in model reactions. Theoretical calculations reveal that the superior performance originates from lattice distortion, a continuous density of states, and an optimized d-band center induced by multi-element incorporation, which promotes the adsorption and conversion of reaction intermediates. The strategies demonstrated in this

work—multi-component synergy, enhanced mass transport via hollow structures, and precise electronic modulation—provide valuable insights for designing highly efficient catalysts for multi-component VOCs oxidation. Future extension to atmospheric pollution control may be realized through compositional screening and surface modification.

4.4 Catalyst's synergistic mechanisms

In the treatment of multi-component VOCs, the synergistic mechanisms of catalysts are complex and multifaceted, primarily manifested through interactions between different active components as well as between active sites and reactant molecules, collectively facilitating efficient VOCs removal. Electronic transfer and lattice oxygen migration between different active components play crucial roles in enhancing overall catalytic performance. In bimetallic catalyst systems, the presence of one metal can promote the dispersion of the other, thereby increasing the number of active sites. For instance, in Pt-Sn bimetallic catalysts, the addition of Sn refines Pt particle size and improves its dispersion on the support, enlarging the active surface area and enhancing VOCs adsorption and activation capacity [147, 152, 153]. Electronic effects also represent a common synergistic mechanism. The mutual influence of electron clouds between different metals alters the electronic structure of active components, thereby modulating the adsorption and activation of reactants. Electron transfer from one metal to another modifies electron density, which in turn adjusts the adsorption strength and reactivity at the active sites. Synergy between active sites and reactant molecules also plays a key role in multi-VOCs control. Cooperative effects between acid sites and redox sites are particularly important for chlorinated VOCs degradation. Acid sites promote C–Cl bond cleavage in chlorinated VOCs, enabling chlorine removal as HCl, while redox sites further oxidize the resulting organic intermediates into harmless products such as CO_2 and H_2O [160]. In the Ru/MoO_x/HZSM-5 catalyst system, the acid sites provided by HZSM-5 effectively adsorb and activate chlorobenzene molecules, promoting C–Cl bond cleavage, while Ru and MoO_x offer redox activity that rapidly oxidizes intermediates, achieving efficient chlorobenzene degradation [150]. Competitive and cooperative adsorption among different active sites also occurs in multi-VOCs systems. Different VOCs molecules compete for active sites on the catalyst surface, where strongly adsorbed species may preferentially occupy sites and influence the adsorption and reaction of others. In certain cases, however, such competitive adsorption can induce synergistic effects—adsorption of one VOCs may modify the electronic or geometric structure of active sites, facilitating the adsorption and reaction of other VOCs [131]. Synergistic interactions also exist between the catalyst support and active components. The support not only disperses the active phase but can also influence its electronic state and catalytic performance through mutual interaction. In CeO_2-supported catalysts, the excellent oxygen storage and release capacity of CeO_2 supplies or stores oxygen species during reaction, cooperating with active components to promote multi-VOCs oxidation. Moreover, strong metal–support interactions between CeO_2 and active species can stabilize the active phase structure, preventing sintering and agglomeration, thereby improving catalyst stability [149, 154, 156].

5 Conclusions and prospects

Over the past decade, the control of mixed air pollutants has evolved from targeting single pollutants toward an integrated, mechanism-driven research paradigm, with catalytic technology emerging as a central pillar in this transition. This review systematically demonstrates that the rational design of catalyst surface active sites, electronic structures, and reaction interfaces enables the synergistic conversion and deep purification of multiple pollutants such as VOCs, NO_x, and O_3. However, a persistent and central challenge remains: the insufficient long-term stability of catalysts under actual complex operating conditions, which severely hinders the translation of synergistic catalysis from the laboratory to engineering applications.

Catalyst deactivation is not caused by a single factor but results from the coupling of multiple mechanisms at physical, chemical, and engineering levels. In practical flue gas or atmospheric environments, processes such as competitive adsorption of water vapor, poisoning by sulfur/chlorine compounds, particulate blockage, thermal sintering, and accumulation of reaction intermediates can all lead to active site masking, structural collapse, or selectivity drift. Particularly for synergistic systems designed to simultaneously treat multiple pollutants, the reaction network is more complex, and unpredictable interactions among different pollutants or between pollutants and catalysts may accelerate deactivation. Therefore, future research must place stability enhancement on an equal or even higher strategic priority than activity optimization.

Looking forward, to enable the large-scale application of synergistic catalytic technology, in-depth exploration should focus on the following directions. First, the rational design of catalysts should shift from "pursuing high initial activity" to "constructing intrinsically robust structures", emphasizing the development of novel materials with enhanced anti-poisoning and anti-sintering capabilities through interfacial engineering, defect anchoring, core-shell structures, and other strategies. Second, it is essential to establish stability evaluation protocols that closely mimic real-world conditions, assessing catalyst performance under harsh scenarios such as dynamic composition, humidity variations, and long-term operation, while employing *in situ* characterization techniques to decipher deactivation kinetics and microscopic mechanisms in real time. Third, active exploration of intelligent integration of catalytic technology with adsorption, plasma, photocatalysis, and other processes should be pursued to construct integrated systems with self-adaptive or self-regenerative functions, thereby alleviating pressure on single catalytic pathways and extending overall service life. Finally, promoting cross-scale research integration-from atomic-level mechanistic insights to particle-scale engineering fabrication and reactor-scale system integration-will ultimately, through lifecycle analysis and AI-assisted optimization, pave a sustainable development path from fundamental research to industrial scale-up. Only by overcoming the stability bottleneck can synergistic catalytic technology truly contribute to future efficient and low-carbon air pollution control systems.

Acknowledgements

This work was financially supported by the National Natural Science Foundation of China (Nos. 52370109 and 52401227), China Postdoctoral Science Foundation (No. 2024M763878), the Natural Science Foundation Project of CQ CSTC (Nos. CSTB2025YITP-QCRCX0064, CSTB2025NSCQ-GPX0827, CSTB2024NSCQ-MSX1045, and CSTB2024NSCQ-MSX0991),

Special Funding for Postdoctoral Research Projects in Chongqing (No. Z39250013), Science and Technology Research Program of Chongqing Municipal Education Commission of China (No. KJZD-M202400802), and the Startup Research Grant (No. F1240093) from Chongqing Jiaotong University.

Declaration of competing interest

All the contributing authors report no conflict of interests in this work.

Author contribution statement

X. X. Z.: Data curation, validation, writing manuscript. Y. H. Z.: Data curation, validation. Y. Y. D.: Project administration, writing manuscript. Y. H. L.: Project administration, funding acquisition, writing-revising manuscript. F. D.: Project administration, funding acquisition. All the authors have approved the final manuscript.

Use of AI statement

During the preparation of this work, the authors used DeepSeek for language polishing. After using this tool, the authors reviewed and edited the content as needed and take full responsibility for the content of the publication.

References

[1] Pfannerstill, E. Y.; Arata, C.;Zhu, Q.; Schulze, B. C.; Ward, R.; Woods, R.;Harkins, C.; Schwantes, R. H.; Seinfeld, J. H.; Bucholtz, A. Temperature-dependent emissions dominate aerosol and ozone formation in Los Angeles. *Science* **2024**, *384*, 1324–1329.

[2] He, C.; Cheng, J.; Zhang, X.; Douthwaite, M.; Pattisson, S.; Hao, Z. Recent advances in the catalytic oxidation of volatile organic compounds: a review based on pollutant sorts and sources. *Chemical Reviews* **2019**, *119*, 4471–4568.

[3] Smith, H. J. Air pollution evolution. *Science* **2018**, *359*, 756–757.

[4] Lewis, A. C.; Carslaw, N.; Marriott, P. J.; Kinghorn, R. M.; Morrison, P.; Lee, A. L.; Bartle, K. D.; Pilling, M. J. A larger pool of ozone-forming carbon compounds in urban atmospheres. *Nature* **2000**, *405*, 778–781.

[5] Kertesz, Z.; Parsons, G. F. Ozone formation in air exposed to cobalt-60 gamma radiation. *Science* **1963**, *142*, 1289–1290.

[6] Chen, Q.; Zeng, Z.; Liu, S.; Zhou, A.; Chen, H.; Zou, Y.; Xu, Y. Diminished lung function mediating the associations between blood levels of volatile organic compounds and respiratory morbidity and mortality. *Scientific Reports* **2025**, *15*, 39488.

[7] Vohra, K.; Marais, E. A.; Bloss, W. J.; Schwartz, J.; Mickley, L. J.; Van Damme, M.; Clarisse, L.; Coheur, P. F. Rapid rise in premature mortality due to anthropogenic air pollution in fast-growing tropical cities from 2005 to 2018. *Science Advances* **2022**, *8*, 4435.

[8] McFiggans, G.; Mentel, T. F.; Wildt, J.; Pullinen, I.; Kang, S.; Kleist, E.; Schmitt, S.; Springer, M.; Tillmann, R.; Wu, C. Secondary organic aerosol reduced by mixture of atmospheric vapours. *Nature* **2019**, *565*, 587–593.

[9] Finlayson-Pitts, B. J.; Pitts Jr, J. N. Tropospheric air pollution: ozone, airborne toxics, polycyclic aromatic hydrocarbons, and particles. *Science* **1997**, *276*, 1045–1051.

[10] Lewis, A. C. The changing face of urban air pollution. *Science* **2018**, *359*, 744–745.

[11] Zhao, M.; Zhang, Y.; Pei, C.; Chen, T.; Mu, J.; Liu, Y.; Wang, Y.; Wang, W.; Xue, L. Worsening ozone air pollution with reduced NO_x and VOCs in the Pearl River Delta region in autumn 2019: Implications for national control policy in China. *Journal of Environmental Management* **2022**, *324*, 116327.

[12] Lee, J. K.; Kwak, M. J.; Jeong, S. G.; Woo, S. Y. Individual and interactive effects of elevated ozone and temperature on plant responses. *Horticulturae* **2022**, *8*, 211.

[13] Feng, Z.; Büker, P.; Pleijel, H.; Emberson, L.; Karlsson, P. E.; Uddling, J. A unifying explanation for variation in ozone sensitivity among woody plants. *Global Change Biology* **2018**, *24*, 78–84.

[14] Sánchez Rodríguez, A. R.; Gómez Álvarez, E.; Méndez, J. M.; Skiba, U. M.; Jones, D. L.; Chadwick, D. R.; Del Campillo, M. C.; Fernandes, R. B.; Kleffmann, J.; Barrón, V. Photocatalytic fixation of NO_x in soils. *Chemosphere* **2023**, *338*, 139576.

[15] Han, Y.; He, M.; Wang, X.; Chen, Q.; Liu, D. Na-doped cobalt-based γ-Al_2O_3 catalysts with enhanced electronic modulation for high NO selectivity in N_2O decomposition. *Industrial & Engineering Chemistry Research* **2025**, 22563–22573.

[16] Li, J.; Deng, S.; Tohti, A.; Li, G.; Yi, X.; Lu, Z.; Liu, J.; Zhang, S. Spatial characteristics of VOCs and their ozone and secondary organic aerosol formation potentials in autumn and winter in the Guanzhong Plain, China. *Environmental Research* **2022**, *211*, 113036.

[17] Bai, J.; Zhang, X.; Wei, Z.; Ma, Y.; Zhang, Q. Constructing N-Pd-O electron bridge between In_2O_3 nanotubes and g-C_3N_4 nanosheets to boost explosive gas sensing performance. *Chemical Engineering Journal* **2024**, *489*, 151321.

[18] Smaiyl, M.; Tulebekov, Y.; Nurpeisov, N.; Satybaldiyev, B.; Snow, D. D.; Uralbekov, B. Human health risk assessment of the photocatalytic oxidation of BTEX over TiO_2/volcanic glass. *Molecules* **2023**, *28*, 8119.

[19] Battista, G.; Lieto Vollaro, E.; Lieto Vollaro, R. Analysis of the main anthropogenic sources' contribution to pollutant emissions in the Lazio Region, Italy. *Applied Sciences* **2021**, *11*, 7936.

[20] Gillani, N. V.; Pleim, J. E. Sub-grid-scale features of anthropogenic emissions of NO_x and VOC in the context of regional Eulerian models. *Atmospheric Environment* **1996**, *30*, 2043–2059.

[21] França Souza, P. A.; Neto, J. L. A.; Cardoso, A. A. A simple technique based on digital images for determination of nitrogen dioxide in ambient air. *Water, Air, & Soil Pollution* **2021**, *232*, 72.

[22] Rosenstiel, T. N.; Potosnak, M. J.; Griffin, K. L.; Fall, R.; Monson, R. K. Increased CO_2 uncouples growth from isoprene emission in an agriforest ecosystem. *Nature* **2003**, *421*, 256–259.

[23] Williams, J.; Fischer, H.; Harris, G.; Crutzen, P.; Hoor, P.; Hansel, A.; Holzinger, R.; Warneke, C.; Lindinger, W.; Scheeren, B. Variability-lifetime relationship for organic trace gases: A novel aid to compound identification and estimation of HO concentrations. *Journal of Geophysical Research: Atmospheres* **2000**, *105*, 20473–20486.

[24] Langner, M.; Draheim, T.; Endlicher, W. Particulate matter in the urban atmosphere: Concentration, distribution, reduction-results of studies in the Berlin metropolitan area. In *Perspectives in urban ecology: ecosystems and interactions between humans and nature in the Metropolis of Berlin* **2011**, 15-41.

[25] Santos, C. Y. M.; Almeida Azevedo, D.; Aquino Neto, F. R. Atmospheric distribution of organic compounds from urban areas near a coal-fired power station. *Atmospheric Environment* **2004**, *38*, 1247–1257.

[26] Deng, H.; Kang, S.; Ma, J.; Wang, L.; Zhang, C.; He, H. Role of structural defects in MnO_x promoted by Ag doping in the catalytic combustion of volatile organic compounds and ambient decomposition of O_3. *Environmental Science & Technology* **2019**, *53*, 10871–10879.

[27] Zhang, K.; Ding, H.; Pan, W.; Mu, X.; Qiu, K.; Ma, J.; Zhao, Y.; Song, J.; Zhang, Z. Research progress of a composite metal oxide catalyst for VOC degradation. *Environmental Science & Technology* **2022**, *56*, 9220–9236.

[28] Munoz, R.; Malhautier, L.; Fanlo, J. L.; Quijano, G. Biological technologies for the treatment of atmospheric pollutants. *International Journal of Environmental Analytical Chemistry* **2015**, *95*, 950–967.

[29] Liu, G.; Tian, Y.; Zhang, B.; Wang, L.; Zhang, X. Catalytic combustion of VOC on sandwich-structured Pt@ZSM-5 nanosheets prepared by controllable intercalation. *Journal of Hazardous Materials* **2019**, *367*, 568–576.

[30] Xiao, M.; Han, D.; Yang, X.; Tchinda, N. T.; Du, L.; Guo, Y.; Wei, Y.; Yu, X.; Ge, M. Ni-doping-induced oxygen vacancy in Pt-CeO_2 catalyst for toluene oxidation: Enhanced catalytic activity, water-resistance, and SO_2-tolerance. *Applied Catalysis B: Environmental* **2023**, *323*, 122173.

[31] Wood, D.; Shaw, S.; Cawte, T.; Shanen, E.; Van Heyst, B. An overview of photocatalyst immobilization methods for air pollution remediation. *Chemical Engineering Journal* **2020**, *391*, 123490.

[32] Rao, Z.; Lu, G.; Chen, L.; Mahmood, A.; Shi, G.; Tang, Z.; Xie, X.; Sun, J. Photocatalytic oxidation mechanism of gas-phase VOCs: Unveiling the role of holes, ·OH and·O_2^-. *Chemical Engineering Journal* **2022**, *430*, 132766.

[33] Sun, M.; Wang, X.; Chen, Z.; Murugananthan, M.; Chen, Y.; Zhang, Y. Stabilized oxygen vacancies over heterojunction for highly efficient and exceptionally durable VOCs photocatalytic degradation. *Applied Catalysis B: Environmental* **2020**, *273*, 119061.

[34] Xu, Z.; Zhang, T.; Lang, J.; Xu, M.; Xie, Y.; Wu, C.; Wang, H.; Yu, H.; Bian, Z. Benzoic acid-mediated oxygen activation for efficient toluene removal on the Co-Vo-Cu catalyst via *in situ* ligand modulation. *Environmental Science & Technology* **2025**, *59*, 15907–15918.

[35] Hu, X.; Liu, B.; Ma, H.; Fang, R.; Zhang, T.; Li, Y.; Rezaei, B.; Dong, F. Spatially separated molecular activation over dual sites in Sn-doped $ZnGa_2O_4/SnO_2$ photocatalysts toward complete VOCs mineralization. *Advanced Science* **2025**, e09891.

[36] Li, J.; Zhu, R.; Cheng, Y.; Lambert, C. K.; Yang, R. T. Mechanism of propene poisoning on Fe-ZSM-5 for selective catalytic reduction of NO_x with ammonia. *Environmental science & technology* **2010**, *44*, 1799–1805.

[37] Han, L.; Cai, S.; Gao, M.; Hasegawa, J. Y.; Wang, P.; Zhang, J.; Shi, L.; Zhang, D. Selective catalytic reduction of NO_x with NH_3 by using novel catalysts: State of the art and future prospects. *Chemical Reviews* **2019**, *119*, 10916–10976.

[38] Li, X.; Ma, J.; He, H. Recent advances in catalytic decomposition of ozone. *Journal of Environmental Sciences* **2020**, *94*, 14–31.

[39] Nicolas, M.; Ndour, M.; Ka, O.; D'Anna, B.; George, C. Photochemistry of atmospheric dust: ozone decomposition on illuminated titanium dioxide. *Environmental science & technology* **2009**, *43*, 7437–7442.

[40] Zhang, Q.; Zheng, Y.; Wang, W.; Wang, Y.; Xue, G.; Gong, C. Performance-enhanced catalysts derived from spent ternary lithium-ion batteries for simultaneous removal of NO_x and VOCs. *Journal of Materials Chemistry A* **2025**, *13*, 1346913481.

[41] Gervasini, A.; Vezzoli, G.; Ragaini, V. VOC removal by synergic effect of combustion catalyst and ozone. *Catalysis Today* **1996**, *29*, 449–455.

[42] Wang, Z.; Liu, Y.; Yang, T.; Deng, J.; Xie, S.; Dai, H. Catalytic performance of cobalt oxide-supported gold-palladium nanocatalysts for the removal of toluene and o-xylene. *Chinese Journal of Catalysis* **2017**, *38*, 207–216.

[43] Fujishima, A.; Honda, K. Electrochemical photolysis of water at a semiconductor electrode. *Nature* **1972**, *238*, 37–38.

[44] Ikhlaq, A.; Kasprzyk-Hordern, B. Catalytic ozonation of chlorinated VOCs on ZSM-5 zeolites and alumina: formation of chlorides. *Applied Catalysis B: Environmental* **2017**, *200*, 274–282.

[45] Shu, Y.; He, M.; Ji, J.; Huang, H.; Liu, S.; Leung, D. Y. Synergetic degradation of VOCs by vacuum ultraviolet photolysis and catalytic ozonation over Mn-xCe/ZSM-5. *Journal of Hazardous Materials* **2019**, *364*, 770–779.

[46] Li, K.; Wang, H.; Chen, L.; Li, J.; Dong, F. Synergistic degradation of NO and C_7H_8 for inhibition of O_3 generation. *Applied Catalysis B: Environmental* **2022**, *312*, 121423.

[47] Dong, C.; Yang, J. J.; Xie, L. H.; Cui, G.; Fang, W. H.; Li, J. R. Catalytic ozone decomposition and adsorptive VOCs removal in bimetallic metal-organic frameworks. *Nature Communications* **2022**, *13*, 4991.

[48] Pan, T.; Deng, H.; Lu, Y.; Ma, J.; Wang, L.; Zhang, C.; He, H. Synergistic catalytic oxidation of typical volatile organic compound mixtures on Mn-based catalysts: significant promotion effect and reaction mechanism. *Environmental Science & Technology* **2022**, *57*, 1123–1133.

[49] Bi, F.; Wei, J.; Gao, B.; Liu, N.; Xu, J.; Liu, B.; Huang, Y.; Zhang, X. New insight into the antagonism mechanism between binary VOCs during their degradation over Pd/ZrO_2 catalysts. *ACS Es&T Engineering* **2024**, *4*, 1346–1355.

[50] Liu, J.; Yang, L.; Dai, Z.; Jiang, W.; Ma, S.; Yao, L.; Chen, Y.; Zhou, Q.; Zheng, J. Zeolite-induced defect engineering for synthesis of CuBTC-derived novel carbon-zeolite bifunctional support catalyst for multicomponent VOCs catalytic oxidation removal. *Chemical Engineering Journal* **2024**, *500*, 156830.

[51] Liu, T.; Jin, Y.; Zhou, B.; Mo, S.; Yang, Z.; Wang, J.; Si, W.; Li, J. Promotion toluene oxidation by NO_x on vanadia-titanium catalysts: Ring-opening mechanism of the key intermediate benzohydroxamic acid. *Applied Catalysis B: Environment and Energy* **2025**, *365*, 124918.

[52] Hu, Y.; Chao, T.; Dou, Y.; Xiong, Y.; Liu, X.; Wang, D. Isolated metal centers activate small molecule electrooxidation: Mechanisms and applications. *Advanced Materials* **2025**, *37*, 2418504.

[53] Wu, Z.; Meng, X.; Zhao, Z. Efficient removal of VOCs enabled by triboelectric-photocatalytic coupling effect. *Nano Energy* **2024**, *132*, 110364.

[54] Witkowski, H.; Jackiewicz Rek, W.; Jarosławski, J.; Chilmon, K.; Szkop, A. Ozone formation during photocatalytic oxidation of nitric oxides under UV irradiation with the use of commercial TiO_2 photocatalytic powders. *Materials* **2022**, *15*, 5905.

[55] Ying, J.; Wang, Y.; Zhang, H.; Bai, Y.; Zhu, J.; Lu, X.; Li, W.; Mu, L. Unraveling humidity's dual effects on trace methane photocatalytic ozonation: Enhanced radical generation versus active site blockade. *Journal of Environmental Chemical Engineering* **2025**, *13*, 120330.

[56] Ma, J.; Chu, B.; Liu, J.; Liu, Y.; Zhang, H.; He, H. NO_x promotion of SO_2 conversion to sulfate: An important mechanism for the occurrence of heavy haze during winter in Beijing. *Environmental Pollution* **2018**, *233*, 662–669.

[57] Gong, Z.; Gu, X.; Li, C.; Zhu, C.; Ning, H.; Tang, R.; Li, J.; Xu, G.; Yu, J. Enhanced dual-active-site VPO-VMoTi tandem catalytic filter for simultaneous removal of NO_x and VOCs at low temperatures. *Chemical Engineering Journal* **2025**, *509*, 161186.

[58] Wang, X.; Mahmood, A.; Lu, G.; Xie, X.; Sun, J. Synergistic photocatalytic treatment of aromatic hydrocarbons/NO_x mixtures over TiO_2: The activation and replenishment of lattice oxygen. *Chemical Engineering Journal* **2022**, *450*, 138168.

[59] Gan, L.; Ye, P.; Tian, X.; Mi, J.; Xing, J.; Xue, Q.; Wu, Q.; Chen, J.; Li, J. Simultaneous removal of NO_x and VOCs by Si doping CeO_2 based catalysts: An acidity and redox properties balance strategy. *Fuel* **2024**, *366*, 131396.

[60] Zheng, F.; Liu, C.; Ma, X.; Zhou, Z.; Lu, J. Review on NH_3-SCR for simultaneous abating NO_x and VOCs in industrial furnaces: catalysts' composition, mechanism, deactivation and regeneration. *Fuel Processing Technology* **2023**, *247*, 107773.

[61] Zhao, H.; Meng, P.; Gao, S.; Wang, Y.; Sun, P.; Wu, Z. Recent advances in simultaneous removal of NO_x and VOCs over bifunctional catalysts via SCR and oxidation reaction. *Science of The Total Environment* **2024**, *906*, 167553.

[62] Guo, Z.; Lin, B.; Huang, Y.; Tang, J.; Chen, P.; Ye, D.; Hu, Y. Design of bimetallic catalyst with dual-functional Cu-Ce sites for synergistic NO_x and toluene abatement. *Applied Catalysis B: Environmental* **2024**, *342*, 123430.

[63] Gan, L.; Li, K.; Xiong, S.; Zhang, Y.; Chen, J.; Peng, Y.; Li, J. MnO_x-CeO_2 catalysts for effective NO_x reduction in the presence of chlorobenzene. *Catalysis Communications* **2018**, *117*, 1–4.

[64] Liang, Y.; Wang, B.; Xuan, Y.; Fan, W.; An, P.; Meng, S.; Zhu, X.; Yun, Y.; Luan, T.; Wang, D. Significant promoting effect of toluene oxidation by CO on $CuMnO_x$ catalysts: Heterostructure and CO co-accelerated active oxygen cycling. *Applied Catalysis B: Environment and Energy* **2025**, *373*, 125325.

[65] Li, J. R.; Zhang, W. P.; Li, C.; He, C. Efficient catalytic degradation of toluene at a readily prepared Mn-Cu catalyst: Catalytic performance and reaction pathway. *Journal of Colloid and Interface Science* **2021**, *591*, 396–408.

[66] Chen, Y.; Chen, Z.; Zhang, C.; Chen, L.; Tang, J.; Liao, Y.; Ma, X. Multiple pollutants control of NO, benzene and toluene from coal-fired plant by Mo/Ni impregnated TiO_2-based NH_3-SCR catalyst: A DFT supported experimental study. *Applied Surface Science* **2022**, *599*, 153986.

[67] Ye, L.; Lu, P.; Xianhui, Y.; Huang, H. Boosting simultaneous catalytic removal of NO_x and toluene via cooperation of Lewis acid and oxygen vacancies. *Applied Catalysis B: Environmental* **2023**, *331*, 122696.

[68] Guo, Y.; Wen, M.; Li, G.; An, T. Recent advances in VOC elimination by catalytic oxidation technology onto various nanoparticles catalysts: a critical review. *Applied Catalysis B: Environmental* **2021**, *281*, 119447.

[69] Chu, P.; Zhang, L.; Wang, Z.; Wei, L.; Liu, Y.; Dai, H.; Guo, G.; Duan, E.; Zhao, Z.; Deng, J. Regulation lattice oxygen mobility via dual single atoms for simultaneously enhancing VOC oxidation and NO_x reduction. *Environmental Science & Technology* **2024**, *58*, 17475–17484.

[70] Wantz, E.; Kane, A.; Lhuissier, M.; Amrane, A.; Audic, J. L.; Couvert, A. A mathematical model for VOCs removal in a treatment process coupling absorption and biodegradation. *Chemical Engineering Journal* **2021**, *423*, 130106.

[71] Dwivedi, P.; Gaur, V.; Sharma, A.; Verma, N. Comparative study of removal of volatile organic compounds by cryogenic condensation and adsorption by activated carbon fiber. *Separation and Purification Technology* **2004**, *39*, 23–37.

[72] Rolewicz Kalińska, A.; Lelicińska Serafin, K.; Manczarski, P. Volatile organic compounds, ammonia and hydrogen sulphide removal using a two-stage membrane biofiltration process. *Chemical Engineering Research and Design* **2021**, *165*, 69–80.

[73] Li, X.; Wang, S.; Zhang, X.; Mei, D.; Xu, Y.; Yu, P.; Sun, Y. Nonthermal plasma catalysis enhances simultaneous removal of toluene and ozone over TiO_2@ZIF-8. *Journal of Cleaner Production* **2022**, *332*, 130107.

[74] Guo, Q.; Zhou, C.; Ma, Z.; Yang, X. Fundamentals of TiO_2 photocatalysis: concepts, mechanisms, and challenges. *Advanced Materials* **2019**, *31*, 1901997.

[75] Lian, Z.; Li, Y.; Shan, W.; He, H. Recent progress on improving low-temperature activity of vanadia-based catalysts for the selective catalytic reduction of NO_x with ammonia. *Catalysts* **2020**, *10*, 1421.

[76] Lin, B.; Guo, Z.; Li, J.; Xiao, G.; Ye, D.; Hu, Y. V-Cu bimetallic oxide supported catalysts for synergistic removal of toluene and NO_x from coal-fired flue gas: The crucial role of support. *Chemical Engineering Journal* **2023**, *458*, 141443.

[77] Long, Y.; Su, Y.; Chen, M.; Lu, S.; Luo, X.; Zhu, Z.; Wu, Z.; Weng, X. Polymerization state of vanadyl species affects the catalytic activity and arsenic resistance of the V_2O_5-WO_3/TiO_2 catalyst in multipollutant control of NO_x and chlorinated aromatics. *Environmental Science & Technology* **2023**, *57*, 7590–7598.

[78] Chen, L.; Liao, Y.; Xin, S.; Song, X.; Liu, G.; Ma, X. Simultaneous removal of NO and volatile organic compounds (VOCs) by Ce/Mo doping-modified selective catalytic reduction (SCR) catalysts in denitrification zone of coal-fired flue gas. *Fuel* **2020**, *262*, 116485.

[79] Lai, J.; Ma, Y.; Wu, J.; Yu, H.; Li, X.; Lin, X. The synergistic catalysis of chloroaromatic organics and NO_x over monolithic vanadium-based catalysts at low temperature. *Catalysts* **2022**, *12*, 1342.

[80] Huang, X.; Wang, D.; Yang, Q.; Peng, Y.; Li, J. Multi-pollutant control (MPC) of NO and chlorobenzene from industrial furnaces using a vanadia-based SCR catalyst. *Applied Catalysis B: Environmental* **2021**, *285*, 119835.

[81] Xiao, G.; Guo, Z.; Lin, B.; Fu, M.; Ye, D.; Hu, Y. Cu-VWT catalysts for synergistic elimination of NO_x and volatile organic compounds from coal-fired flue gas. *Environmental Science & Technology* **2022**, *56*, 10095–10104.

[82] Li, G.; Shen, K.; Wang, L.; Zhang, Y.; Yang, H.; Wu, P.; Wang, B.; Zhang, S. Synergistic degradation mechanism of chlorobenzene and NO_x over the multi-active center catalyst: The role of NO_2, Brønsted acidic site, oxygen vacancy. *Applied Catalysis B: Environmental* **2021**, *286*, 119865.

[83] Pan, H.; Chen, Z.; Feng, X.; Cao, S.; Jian, Y.; Chen, J.; He, C. Sulfur-resistant mechanism of MnO_x@CeO_2@MgO core-shell catalyst in simultaneous removal of NO_x and chlorobenzene. *Applied Catalysis B: Environment and Energy* **2025**, *362*, 124761.

[84] Lin, B.; Tang, J.; Yang, J.; Fu, M.; Ye, D.; Hu, Y. Insight to the cooperation between electronic unsaturated metal sites and hydroxyl species improves the SO_2 resistance of Fe-MnO_2@TiO_2 for simultaneous removal of toluene and NO. *Applied Catalysis B: Environment and Energy* **2025**, *361*, 124619.

[85] Jia, X.; Yu, C.; Fang, H.; Hou, D.; Wang, J.; Zhang, Y.; Zhu, F.; Xiong, J.; Dan, J.; He, D. MnO_x catalysts with different morphologies for low temperature synergistic removal of NO_x and toluene: structure-activity relationship and mutual inhibitory effects. *Journal of Environmental Chemical Engineering* **2022**, *10*, 108646.

[86] Lin, B.; Guo, Z.; Tang, J.; Chen, P.; Ye, D.; Hu, Y. Modulating the microstructure and surface acidity of MnO_2 by doping-induced phase transition for simultaneous removal of toluene and NO_x at low temperature. *Environmental Science & Technology* **2024**, *58*, 10398–10408.

[87] Kang, D.; Shi, Q.; Zhang, C.; Zhao, P.; Lyu, H.; Yang, M.; Bian, Y.; Shen, B. Synergistic removal of NO_x and CB by Co-MnO_x catalysts in a low-temperature window. *Chemical Engineering Journal* **2023**, *476*, 146369.

[88] Ma, S.; Peng, K.; Ji, H.; Hou, Y.; Li, Y.; Huang, Z. Synergistic removal of nitrogen oxides and toluene and their interaction mechanism on Cu-MnO_2 catalyst. *Fuel* **2025**, *379*, 133009.

[89] Ma, S.; Hou, Y.; Yang, Y.; Li, Y.; Li, B.; Cui, Y.; Chen, H.; Huang, Z. Mechanism of SO_2 effect on the simultaneous removal of NO_x and propane over bifunctional $NiMn_2O_4$-CeO_2 catalysts. *Journal of Hazardous Materials* **2024**, *480*, 136473.

[90] Sun, C.; Ye, L.; Lu, P.; Yan, X.; Huang, J.; Tang, Z.; Chen, D.; Cen, C. Synergistic removal of acetone and NO_x by Ag modified Mn/HZSM-5 catalyst. *Chemical Engineering Journal* **2025**, *505*, 159622.

[91] Chen, Z.; Zhao, C.; Wei, N.; Yun, J.; Chu, R.; Zheng, H.; Feng, X.; Tong, Z.; Chen, Z. New insights and reaction mechanisms in the design of catalysts for the synergistic removal of NO_x and VOCs from coke oven flue gas: Dual regulation of oxidative properties and acidic sites. *Journal of Hazardous Materials* **2024**, *477*, 135052.

[92] Wang, F.; Chen, A.; Lan, T.; Chen, X.; Wang, M.; Hu, X.; Wang, P.; Cheng, D.; Zhang, D. Synergistic catalytic removal of NO_x and chlorinated organics through the cooperation of different active sites. *Journal of Hazardous Materials* **2024**, *468*, 133722.

[93] Ma, J.; Wang, J.; Yuan, J.; Liu, X.; Yang, Y.; Yu, F. The regulating strategy of hierarchical structure and acidity in zeolites and application of gas adsorption: A review. *Chinese Chemical Letters* **2024**, *35*, 109693.

[94] Jia, L.; Liu, J.; Cheng, H.; Zhao, Z.; Liu, J. Review of Core-shell structure zeolite-based catalysts for NO_x emission control. *Journal of Environmental Sciences* **2025**, *150*, 451–465.

[95] Chuang, K. H.; Liu, Z. S.; Chang, Y. H.; Lu, C. Y.; Wey, M. Y. Study of SBA-15 supported catalysts for toluene and NO removal: the effect of promoters (Co, Ni, Mn, Ce). *Reaction Kinetics, Mechanisms and Catalysis* **2010**, *99*, 409–420.

[96] Jiang, S.; Zhang, L.; Zhao, L.; Zhang, J.; Huang, Y. Unveiling mechanism and the roles of distinct active sites over Cu/Beta@CeO_2 with strong core-shell interface interaction for simultaneous removal of NO and toluene. *Chemical Engineering Journal* **2023**, *474*, 145979.

[97] Li, H.; Wei, L.; Liu, Y.; Wang, Z.; Dai, H.; Deng, J. Synergistic removal of NO and chlorinated organics on CeO_2-based catalysts. *Environmental Functional Materials* **2023**, *2*, 57–65.

[98] Wei, L.; Liu, Y.; Dai, H.; Cui, S.; Wang, C.; Hsi, H. C.; Duan, E.; Peng, Y.; Deng, J. Electronic structure tailoring of Al^{3+}-and Ta^{5+}-doped CeO_2 for the synergistic removal of NO and chlorinated organics. *Applied Catalysis B: Environmental* **2022**, *304*, 120939.

[99] Liu, H.; Chen, J.; Wang, Y.; Yin, R.; Yang, W.; Wang, G.; Si, W.; Peng, Y.; Li, J. Interaction mechanism for simultaneous elimination of nitrogen oxides and toluene over the bifunctional CeO_2-TiO_2 mixed oxide catalyst. *Environmental Science & Technology* **2022**, *56*, 4467–4476.

[100] Li, Y.; Sun, Z.; Zhang, Z.; Niu, X.; Zhu, Y. Enhancing reactive oxygen release-replenishment and Lewis acid acidity by Nb doping in $NbmCeO_x$ for simultaneous elimination of NO_x and toluene. *Applied Catalysis B: Environment and Energy* **2025**, *364*, 124842.

[101] Zhang, T.; Jiang, J.; Sun, W.; Gong, S.; Liu, X.; Tian, Y.; Wang, D. Spatial configuration of Fe-Co dual-sites boosting catalytic intermediates coupling toward oxygen evolution reaction. *Proceedings of the National Academy of Sciences* **2024**, *121*, e2317247121.

[102] Han, L.; Song, Y.; Zhang, H.; Wang, F.; Yu, H.; Zhang, J.; Peng, D.; Hu, X.; Xie, M.; Zhang, D. Synergistic catalytic elimination of NO_x and CH_3SH in CaO-containing flue gases. *ACS ES&T Engineering* **2025**, 2108-2117.

[103] Liu, T.; Liu, T.; Wang, B.; Si, W.; Wang, J.; Li, J. Relieved toluene ammoxidation by Cu regulated pd orbital coupling in $CuVO_x$/TiO_2 for enhanced synergistic elimination of NO_x and VOCs. *Journal of Environmental Chemical Engineering* **2025**, 118209.

[104] Gao, X.; Du, X.; Fu, Y.; Mao, J.; Luo, Z.; Ni, M.; Cen, K. Theoretical and experimental study on the deactivation of V_2O_5 based catalyst by lead for selective catalytic reduction of nitric oxides. *Catalysis Today* **2011**, *175*, 625–630.

[105] Weng, X.; Xue, Y.; Chen, J.; Meng, Q.; Wu, Z. Elimination of chloroaromatic congeners on a commercial V_2O_5-WO_3/TiO_2 catalyst: The effect of heavy metal Pb. *Journal of Hazardous Materials* **2020**, *387*, 121705.

[106] Qi, L.; Li, J.; Yao, Y.; Zhang, Y. Heavy metal poisoned and regeneration of selective catalytic reduction catalysts. *Journal of Hazardous Materials* **2019**, *366*, 492–500.

[107] Peng, Y.; Li, J.; Si, W.; Luo, J.; Dai, Q.; Luo, X.; Liu, X.; Hao, J. Insight into deactivation of commercial SCR catalyst by arsenic: an experiment and DFT study. *Environmental Science & Technology* **2014**, *48*, 13895–13900.

[108] Long, Y.; Su, Y.; Xue, Y.; Wu, Z.; Weng, X. V_2O_5-WO_3/TiO_2 catalyst for efficient synergistic control of NO_x and chlorinated organics: Insights into the arsenic effect. *Environmental Science & Technology* **2021**, *55*, 9317–9325.

[109] Song, Z.; Yu, S.; Liu, H.; Wang, Y.; Gao, C.; Wang, Z.; Qin, Y.; Peng, Y.; Li, J. Carbon/chlorinate deposition on MnO_x-CeO_2 catalyst in chlorobenzene combustion: The effect of SCR flue gas. *Chemical Engineering Journal* **2022**, *433*, 133552.

[110] Wang, Q.; Lin, F.; Zhou, J.; Zhang, J.; Jin, J. Effect of HCl and o-DCBz on NH_3-SCR of NO over MnO_x/TiO_2 and MnO_x-CeO_2/TiO_2 catalysts. *Applied Catalysis A: General* **2020**, *605*, 117801.

[111] Liu, J.; Dai, X.; Wu, Z.; Weng, X. Unveiling the secondary pollution in the catalytic elimination of chlorinated organics: The formation of dioxins. *Chinese Chemical Letters* **2020**, *31*, 1410–1414.

[112] Ilmasani, R. F.; Yao, D.; Ho, P. H.; Bernin, D.; Creaser, D.; Olsson, L. Deactivation of phosphorus-poisoned Pd/SSZ-13 for the passive adsorption of NO_x. *Journal of Environmental Chemical Engineering* **2022**, *10*, 107608.

[113] Cao, P.; Mu, X.; Chen, F.; Wang, S.; Liao, Y.; Liu, H.; Du, Y.; Li, Y.; Peng, Y.; Gao, M. Breaking symmetry for better catalysis: insights into single-atom catalyst design. *Chemical Society Reviews* **2025**, *54*, 3848–3905.

[114] Yang, H.; Duan, P.; Zhuang, Z.; Luo, Y.; Shen, J.; Xiong, Y.; Liu, X.; Wang, D. Understanding the dynamic evolution of active sites among single atoms, clusters, and nanoparticles. *Advanced Materials* **2025**, *37*, 2415265.

[115] Liu, H.; Zhang, Y.; Liu, Z.; Wang, S.; Mu, X.; Zhang, Q.; Cao, W.; Liu, S.; Wang, D.; Dai, Z. Grain boundary-driven synergistic dual-mechanism catalysis in RuO_2 for enhancing acidic oxygen evolution reaction activity and stability. *Journal of the American Chemical Society* **2025**, 44141-44151.

[116] Li, X.; Yu, J.; Jaroniec, M. Hierarchical photocatalysts. *Chemical Society Reviews* **2016**, *45*, 2603–2636.

[117] Li, X.; Wang, C.; Tang, J. Methane transformation by photocatalysis. *Nature Reviews Materials* **2022**, *7*, 617–632.

[118] Nolan, M.; Iwaszuk, A.; Lucid, A. K.; Carey, J. J.; Fronzi, M. Design of novel visible light active photocatalyst materials: surface modified TiO_2. *Advanced Materials* **2016**, *28*, 5425–5446.

[119] Kask, M.; Bolobajev, J.; Krichevskaya, M. Gas-phase photocatalytic degradation of acetone and toluene, and their mixture in the presence of ozone in continuous multi-section reactor as possible air post-treatment for exhaust from pulsed corona discharge. *Chemical Engineering Journal* **2020**, *399*, 125815.

[120] Sui, Y.; Sun, X.; Guan, J.; Chen, Z.; Zhu, X.; Lou, X.; Li, X.; Shen, J.; Liu, X.; Zhang, X. Kill two birds with one stone: simultaneous removal of volatile organic compounds and ozone secondary pollution by a novel photocatalytic process. *RSC Advances* **2024**, *14*, 14784–14792.

[121] Koppenol, W. The reduction potential of the couple $O_3/O^{\cdot}_3^-$: Consequences for mechanisms of ozone toxicity. *FEBS Letters* **1982**, *140*, 169-172.

[122] Zhang, Z.; Lin, F.; Xiang, L.; Yu, H.; Wang, Z.; Yan, B.; Chen, G. Synergistic effect for simultaneously catalytic ozonation of chlorobenzene and NO over $MnCoO_x$ catalysts: Byproducts formation under practical conditions. *Chemical Engineering Journal* **2022**, *427*, 130929.

[123] Altof, K.; Krichevskaya, M.; Preis, S.; Tähemaa, T.; Bolobajev, J. Ozone-assisted degradation of 2-methoxyethanol in a prototype plug flow photocatalytic reactor. *Chemical Engineering Journal* **2024**, *481*, 148488.

[124] Wu, M.; Kwok, Y. H.; Zhang, Y.; Szeto, W.; Huang, H.; Leung, D. Y. Synergetic effect of vacuum ultraviolet photolysis and ozone catalytic oxidation for toluene degradation over MnO_2-rGO composite catalyst. *Chemical Engineering Science* **2021**, *231*, 116288.

[125] Payan, A.; Aghdam, N. C.; Soltan, J. Catalytic oxidation of acetone in air over Ag modified CeO_2 catalysts under VUV irradiation: Comparison of different treatment process, performance, and mechanism studies. *Journal of Environmental Chemical Engineering* **2022**, *10*, 107253.

[126] Payan, A.; Jafarihaghighi, F.; Soltan, J. Boosting catalytic activity of Ag-modified CeO_2-Al_2O_3 mixed metal oxide support via coupling with a VUV photoreactor: A catalytic ozonation system applied towards VOC oxidation. *Applied Catalysis A: General* **2025**, 120370.

[127] Payan, A.; Jafarihaghighi, F.; Soltan, J. Enhanced catalytic performance of α-MnO_2 via coupling with a vacuum ultraviolet photoreactor: A catalytic ozonation approach targeting VOC oxidation. *Process Safety and Environmental Protection* **2025**, 107499.

[128] Wang, H.; Huang, Z.; Jiang, Z.; Jiang, Z.; Zhang, Y.; Zhang, Z.; Shangguan, W. Trifunctional C@MnO catalyst for enhanced stable simultaneously catalytic removal of formaldehyde and ozone. *ACS Catalysis* **2018**, *8*, 3164–3180.

[129] Ma, W.; Feng, Z.; Chen, X.; Xia, M.; Liu, Y.; Zhang, Y.; Liu, Y.; Wang, Y.; Zheng, F.; Hua, C. Overlooked significance of reactive chlorines in the reacted loss of VOCs and the formation of O_3 and SOA. *Environmental Science & Technology* **2025**, *59*, 6155–6166.

[130] Li, X.; Zhang, L.; Yang, Z.; Wang, P.; Yan, Y.; Ran, J. Adsorption materials for volatile organic compounds (VOCs) and the key factors for VOCs adsorption process: A review. *Separation and Purification Technology* **2020**, *235*, 116213.

[131] Zhang, X.; Gao, B.; Creamer, A. E.; Cao, C.; Li, Y. Adsorption of VOCs onto engineered carbon materials: A review. *Journal of Hazardous Materials* **2017**, *338*, 102–123.

[132] An, Y.; Fu, Q.; Zhang, D.; Wang, Y.; Tang, Z. Performance evaluation of activated carbon with different pore sizes and functional groups for VOC adsorption by molecular simulation. *Chemosphere* **2019**, *227*, 9–16.

[133] Yue, Z.; Vakili, A.; Wang, J. Activated carbon fibers from meltblown isotropic pitch fiber webs for vapor phase adsorption of volatile organic compounds. *Chemical Engineering Journal* **2017**, *330*, 183–190.

[134] Guo, X.; Li, D.; Wang, L.; Deng, H.; Wang, Y.; Wang, H.; Ma, J.; Yu, Y.; He, H. Adsorption performance and mechanism of methanol by H-ZSM-5, H-Beta, and H-SSZ-13 zeolites. *Separation and Purification Technology* **2025**, *361*, 131634.

[135] Liu, X.; Chee, S. W.; Raj, S.; Sawczyk, M.; Král, P.; Mirsaidov, U. Three-step nucleation of metal-organic framework nanocrystals. *Proceedings of the National Academy of Sciences* **2021**, *118*, e2008880118.

[136] Kampouraki, Z. C.; Giannakoudakis, D. A.; Nair, V.; Hosseini Bandegharaei, A.; Colmenares, J. C.; Deliyanni, E. A. Metal organic frameworks as desulfurization adsorbents of DBT and 4,6-DMDBT from fuels. *Molecules* **2019**, *24*, 4525.

[137] Chen, J.; Zhang, R.; Guo, S.; Pan, Y.; Nezamzadeh Ejhieh, A.; Lan, Q. Metal-organic frameworks (MOFs): A review of volatile organic compounds (VOCs) detection. *Talanta* **2025**, *286*, 127498.

[138] Qin, J.; Yang, J.; Huang, H.; Fu, M.; Ye, D.; Hu, Y. Tuning the hierarchical pore structure and the metal site in a metal-organic framework derivative to unravel the mechanism for the adsorption of different volatile organic compounds. *Environmental Science & Technology* **2023**, *57*, 15703–15714.

[139] Zhang, M.; Zhu, W.; Liu, Z.; Chen, S.; Zhou, D.; Mu, X.; Zhuang, Z.; Wang, S.; Yang, J.; Du, Y. Selective sieving effect of multi-atomic bismuth interfaces for efficient formate electrosynthesis and evolution at industrial current density. *Angewandte Chemie* **2025**, *137*, e202510206.

[140] Du, Y.; Mu, X.; Wang, S.; Zhang, Y.; Chen, F.; Zhang, M.; Li, J.; Cao, P.; Yuan, J.; Zhang, Y. Atomically dispersed catalysts: for the efficient and stable industrial electrosynthesis of H_2O_2. *Energy & Environmental Science* **2025**, 5833–5867.

[141] Li, J.; Chen, R.; Cui, W.; Dong, X.; Wang, H.; Kim, K. H.; Chu, Y.; Sheng, J.; Sun, Y.; Dong, F. Synergistic photocatalytic decomposition of a volatile organic compound mixture: high efficiency, reaction mechanism, and long-term stability. *ACS Catalysis* **2020**, *10*, 7230–7239.

[142] Wu, X.; Lin, Y.; Wang, Y.; Wu, S.; Yang, C. Volatile organic compound removal via biofiltration: influences, challenges, and strategies. *Chemical Engineering Journal* **2023**, *471*, 144420.

[143] Wei, T.; Ma, C.; Wen, Y.; Yue, H.; Yang, S.; Zhao, J.; Zhang, S.; Li, W.; Li, S.; Wang, X. An integrated biological system for air pollution control in WtE plants and interaction between NO reduction and toluene oxidation. *Journal of Cleaner Production* **2022**, *355*, 131792.

[144] González Martín, J.; Cantera, S.; Muñoz, R.; Lebrero, R. Indoor air VOCs biofiltration by bioactive coating packed bed bioreactors. *Journal of Environmental Management* **2024**, *349*, 119362.

[145] Han, M. F.; Hu, X. R.; Wang, Y. C.; Tong, Z.; Wang, C.; Cheng, Z. W.; Feng, K.; Qu, M. M.; Chen, J. M.; Deng, J. G. Comparison of separated and combined photodegradation and biofiltration technology for the treatment of volatile organic compounds: A critical review. *Critical Reviews in Environmental Science and Technology* **2022**, *52*, 1325–1355.

[146] Tian, R.; Lu, J.; Xu, Z.; Zhang, W.; Liu, J.; Wang, L.; Xie, Y.; Zhao, Y.; Cao, X.; Luo, Y. Unraveling the synergistic reaction and the deactivation mechanism for the catalytic degradation of double components of sulfur-containing VOCs over ZSM-5-based materials. *Environmental Science & Technology* **2022**, *57*, 1443–1455.

[147] Gao, R.; Zhang, M.; Liu, Y.; Xie, S.; Deng, J.; Ke, X.; Jing, L.; Hou, Z.; Zhang, X.; Liu, F. Engineering platinum catalysts via a site-isolation strategy with enhanced chlorine resistance for the elimination of multicomponent VOCs. *Environmental Science & Technology* **2022**, *56*, 9672–9682.

[148] Feng, Y.; Wei, L.; Liu, Y.; Dai, H.; Zhao, Z.; Deng, J. Rapid supplement of active oxygen by constructing Pt-Fe alloy structure to improve catalytic stability for furniture paints industry VOCs removal. *Separation and Purification Technology* **2023**, *324*, 124621.

[149] Wang, J.; Liu, Y.; Deng, J.; Jing, L.; Hao, X.; Gao, R.; Dai, H. Highly efficient catalytic ozonization at ultralow temperatures of multicomponent VOCs over the Pt/CeO_2 catalysts. *ACS ES&T Engineering* **2023**, *4*, 419–432.

[150] Wu, L.; Liu, Y.; Yu, X.; Gao, R.; Jia, Y.; Sun, Q.; Feng, Y.; Jing, L.;

Hou, Z.; Deng, J. Constructing bridge hydroxyl groups on the Ru/MO_x/HZSM-5 (M=W, Mo) catalysts to promote the hydrolysis oxidation of multicomponent VOCs. *Environmental Science & Technology* **2024**, *59*, 945–955.

[151] He, T.; Li, G.; Ji, J.; Liu, W.; Zhang, H.; Xie, X.; Huang, S.; Huang, T.; Peng, H. Tailored engineering of intracrystalline mesopores for boosting multicomponent volatile organic compounds simultaneous deep oxidation. *Applied Catalysis B: Environment and Energy* **2025**, *362*, 124752.

[152] Li, Z.; Gao, R.; Hou, Z.; Yu, X.; Dai, H.; Deng, J.; Liu, Y. Tandem supported Pt and ZSM-5 catalyst with separated catalytic functions for promoting multicomponent VOCs oxidation. *Applied Catalysis B: Environmental* **2023**, *339*, 123131.

[153] Gao, R.; Tian, X.; Ding, X.; Hou, Z.; Li, Z.; Yu, X.; Wang, J.; Wu, L.; Jing, L.; Deng, J. Regulating catalytic stability of PtSnM/CeO_2 (M=Mn, W, Nb) catalysts via the closely coupled multi-active sites to promote multicomponent VOCs oxidation. *Chemical Engineering Journal* **2023**, *471*, 144456.

[154] Long, Y.; Meng, Q.; Chen, M.; Luo, X.; Dai, Q.; Lu, H.; Wu, Z.; Weng, X. Selective Ru adsorption on SnO_2/CeO_2 mixed oxides for efficient destruction of multicomponent volatile organic compounds: from laboratory to practical possibility. *Environmental Science & Technology* **2022**, *56*, 9762–9772.

[155] Feng, Y.; Wang, C.; Wang, C.; Huang, H.; Hsi, H. C.; Duan, E.; Liu, Y.; Guo, G.; Dai, H.; Deng, J. Catalytic stability enhancement for pollutant removal via balancing lattice oxygen mobility and VOCs adsorption. *Journal of Hazardous Materials* **2022**, *424*, 127337.

[156] Gao, H.; Song, Z.; Mao, Y.; Fan, Y.; Li, R.; Chen, X.; Liu, W.; Zhang, J.; Huang, Z.; Zhang, X. Tight coupling of oxygen vacancies and acidity on α-MnO2 through cerium doping engineering for efficient removal of multi-component VOCs. *Applied Catalysis B: Environment and Energy* **2025**, *362*, 124745.

[157] Xie, X.; Xiang, Y.; Cao, J.; Dai, W.; Ao, Z.; Huang, H.; Yang, X.; Xiao, F.; Ye, X. High-efficiency destruction of aromatic VOC mixtures in a MoS_2 cocatalytic Fe^{3+}/PMS reaction. *Separation and Purification Technology* **2023**, *305*, 122444.

[158] Guo, Y.; Wen, M.; Song, S.; Liu, Q.; Li, G.; An, T. Enhanced catalytic elimination of typical VOCs over $ZnCoO_x$ catalyst derived from *in situ* pyrolysis of ZnCo bimetallic zeolitic imidazolate frameworks. *Applied Catalysis B: Environmental* **2022**, *308*, 121212.

[159] Lei, Y.; Shang, H.; Li, G.; Zhang, L.; Sun, Z.; Wang, X.; Zhao, Y.; Xiang, X.; Zheng, Z.; Pang, X. Synthesis of noble metal-free monodisperse high-entropy oxides hollow nanocubes libraries via a coordination etching strategy. *Nature Communications* **2025**, *16*, 9817.

[160] Su, Y.; Fu, K.; Pang, C.; Zheng, Y.; Song, C.; Ji, N.; Ma, D.; Lu, X.; Liu, C.; Han, R. Recent advances of chlorinated volatile organic compounds' oxidation catalyzed by multiple catalysts: Reasonable adjustment of acidity and redox properties. *Environmental Science & Technology* **2022**, *56*, 9854–9871.